Phonon-assisted optical absorption in germanium

José Menéndez,[1] David J. Lockwood,[2] Joanne C. Zwinkels,[2] and Mario Noël[2]
[1]*Department of Physics, Arizona State University, Tempe, Arizona 85287-1504, USA*
[2]*Metrology Research Center, National Research Council, Ottawa, Ontario, Canada KIA 0R6*

(Received 14 July 2018; published 31 October 2018)

A comprehensive experimental and theoretical study of indirect gap optical absorption in bulk Ge is presented. While this topic has been the subject of intense studies from the early days of semiconductor physics, the resonant aspect of the absorption received very little attention until now. This is a unique property of Ge related to the proximity of the direct and indirect gaps. The absorption coefficient was measured over the entire spectral range between the two gaps for comparison with theory. It is shown that the standard textbook expressions, obtained by assuming intermediate states with constant energy, are in very poor agreement with experiment. A theory first proposed by Hartman [R. L. Hartman, Phys. Rev. **127**, 765 (1962)], which takes into account the energy dependence of the intermediate states, provides a much better account of the photon-energy dependence of the absorption, but the prediction of the experimental absorption strength requires the incorporation of excitonic effects. The latter, however, have only been considered by Elliott [R. J. Elliott, Phys. Rev. **108**, 1384 (1957)] in the limit of constant intermediate state energy. A generalization to the case of energy-dependent intermediate states, consistent with Hartman's theory, is presented here. The basic qualitative difference with the classical Elliott theory is that the excitonic character of the intermediate states affects the computed absorption, generating an additional resonant enhancement that is confirmed by the experimental data. The generalized theory presented here agrees very well with the experimental absorption using independently determined band structure parameters.

DOI: 10.1103/PhysRevB.98.165207

I. INTRODUCTION

The absorption coefficient of indirect gap semiconductors—including its spectral dependence—has recently become the subject of intense theoretical efforts, following advances that make it possible to attempt its calculation from first principles [1–3]. In the case of Si, the energy range between the indirect and direct gaps is of foremost practical interest, since it overlaps with the visible optical absorption that underpins its photovoltaic applications. Germanium, on the other hand, represents a formidable theoretical challenge because the indirect gap energy is only ∼0.1 eV below the lowest direct optical transitions. These transitions appear as intermediate states in perturbation theory expansions of the absorption coefficient, and therefore realistic *ab initio* predictions require the ability to reproduce band dispersions with meV accuracy, a difficult task even for state-of-the-art band structure calculation methods [4]. The unique resonant character of indirect absorption in Ge was recognized as early as 1962 by Hartman, who computed the absorption coefficient without relying on the standard textbook assumption of constant intermediate state energy [5]. However, Hartman did not compare his expressions with experimental data. Furthermore, the available experimental results are not fully satisfactory when it comes to this comparison, since the classic papers [6–8] reporting indirect absorption in Ge made a number of *ad hoc* assumptions regarding the energy dependence of the reflectivity which do not apply to the entire spectral range between the indirect and direct gaps.

Recently identified optoelectronic applications of Ge and related GeSn alloys [9–12] add a new urgency to the need of addressing the poorly understood aspects of indirect absorption in Ge. In a recent Rapid Communication, we presented experimental absorption data for this material and compared with theoretical expressions [13]. A major finding of this work, hereafter referred to as I, is that excitonic effects must be included in the comparison between theory and experiment. For this, an alternative theoretical model was introduced, since the standard theory of excitonic enhancements due to Elliott [14] breaks down when intermediate states cannot be assumed to have a constant energy. In this associated article we present an extended set of experimental reflectivity and absorption data for Ge, further validating the experimental results in I. We also provide full details on the resonant excitonic enhancement model needed to describe the experimental data.

The excitonic structure of band edge absorption in Ge has been studied with exquisite detail [15,16], and theoretical models that take into account the complexities of the conduction and valence bands have been shown to be in remarkable agreement with experimental data [17,18]. However, these models are limited to the band edge, as their extension to the entire spectral range between the indirect and direct edges is not straightforward. Excitonic effects can be computed *ab initio* using the Bethe-Salpeter formalism [19], but this approach does not usually lend itself to implementation in fitting routines running on personal computers. In addition, as indicated above, the accuracy needed for the underlying band structure is difficult to attain. The Elliott model mentioned above makes the drastic approximation of considering isotropic parabolic bands [14]. This leads to simple theoretical expressions, which could be used to correct the absorption

calculated with the Hartman model. However, such approach would be inconsistent, since it would include the energy dependence of the intermediate states at the free electron-hole pair level but neglect it in computing excitonic effects. By contrast, our resonant exciton model treats the intermediate states at the same level as in the Hartman model, while making the same approximations as Elliott [14] regarding band dispersions. This refinement leads to unique physics that is discussed in detail below. The absorption expressions derived here are, as expected, more complex than in the Elliott case, but the calculations can be carried on personal computers, thereby lending themselves to fits of experimental data. As already shown in I, excellent agreement between theory and experiment is obtained at intermediate energies between the indirect and the direct gaps using the deformation potential that couples the two lowest conduction band valleys as the only adjustable parameter. The fit value is found to be in excellent agreement with other independent measurements of this quantity. In this article we also investigate how the approximations made affect the modeling at the absorption edge.

The remainder of the paper is organized as follows. In Sec. II we describe the theory of resonant excitonic indirect absorption. Since a key aspect of the comparison between theory and experiment is the use of absolute values of the absorption, special care is devoted to the definition of all parameters and prefactors needed for the calculation, which are not always used consistently in the literature. Explicit expressions for the absorption coefficient are derived that allow a direct comparison with experiment, and a detailed discussion of the approximations involved is provided. We also show how the Elliott excitonic model and the absorption expressions that ignore the excitonic interaction are obtained as appropriate limits of our model. In Sec. III we discuss our experimental method and present absorption and reflectivity data for samples with different thicknesses. This allows us to investigate not only the most resonant energy range between the indirect and direct gaps, as in I, but also to study the onset of absorption very close to the indirect gap. In Sec. IV we compare theory and experiment, and in Sec. V we discuss our findings and outline future challenges.

II. THEORY

A. Basic absorption expressions

Figure 1 shows schematically the band structure of Ge. The top of the valence band, where we choose the zero of energy, consists of light and heavy holes that are degenerate at the Γ point of the Brillouin zone (BZ). The spin-degenerate conduction band has a local minimum at the Γ point with an energy E_0 above the top of the valence band. The Γ-point conduction band states have s-like character and can be denoted as

$$|S\sigma\rangle; \quad \sigma = \uparrow, \downarrow, \tag{1}$$

where σ indicates the spin degree of freedom. The absolute minimum of the conduction band, at an energy $E_{\rm ind}$ (the indirect gap) is a spin-degenerate state at the L point of the BZ. The valence band wave functions at the Γ point are p-like. Their sixfold degeneracy is lifted by the spin-orbit interaction. We ignore the split-off band here because the spin-orbit splitting is $\Delta_0 \sim 0.3$ eV, so this band is not involved in the resonant indirect absorption processes that are the focus of this paper. Choosing Cartesian axes, the remaining states can be written as [20]

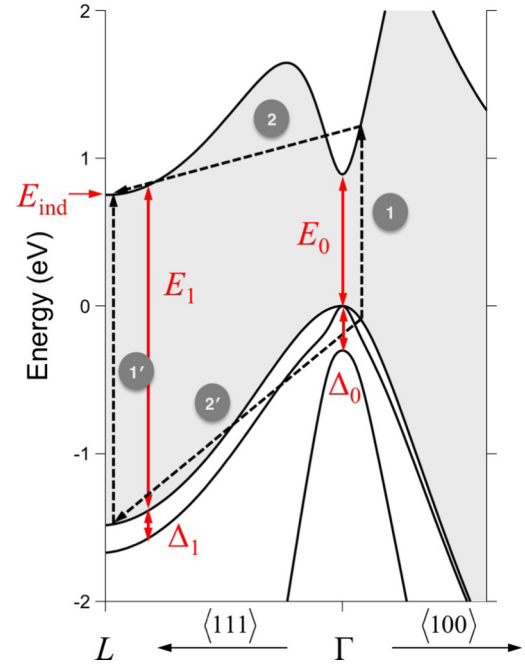

FIG. 1. Band structure of Ge showing important transition energies and splittings (in red) and indirect absorption mechanisms. The sequence 1/2 is the dominant contribution to resonant indirect absorption because the intermediate and final states have similar energies. The sequence 1′/2′ is far less resonant because the intermediate state energy is much larger.

$$\begin{aligned}
|1\rangle &= |HH1\rangle = \left|\frac{3}{2};\frac{3}{2}\right\rangle = -\frac{(|X\uparrow\rangle + i|Y\uparrow\rangle)}{\sqrt{2}},\\
|2\rangle &= |LH1\rangle = \left|\frac{3}{2};\frac{1}{2}\right\rangle = -\frac{(|X\downarrow\rangle + i|Y\downarrow\rangle)}{\sqrt{6}} + \frac{\sqrt{2}|Z\uparrow\rangle}{\sqrt{3}},\\
|3\rangle &= |HH2\rangle = \left|\frac{3}{2};-\frac{3}{2}\right\rangle = \frac{(|X\downarrow\rangle - i|Y\downarrow\rangle)}{\sqrt{2}},\\
|4\rangle &= |LH2\rangle = \left|\frac{3}{2};-\frac{1}{2}\right\rangle = \frac{(|X\uparrow\rangle - i|Y\uparrow\rangle)}{\sqrt{6}} + \frac{\sqrt{2}|Z\downarrow\rangle}{\sqrt{3}},
\end{aligned} \tag{2}$$

where the X, Y, Z transform as the coordinates and the wave vector $\boldsymbol{k}$ is along the z direction. In both Eqs. (1) and (2) the spin direction corresponds to the z axis. The bands are assumed to have parabolic dispersion with effective masses $m_\nu (\nu = 1, 2, 3, 4)$ with $m_1 = m_3 = m_{hh}$ (heavy hole) and $m_2 = m_4 = m_{lh}$ (light hole). Corrections for band warping are incorporated into the definition of the effective masses, as discussed in Appendix B. Nonparabolicity is ignored.

Optical absorption across the indirect gap requires the combined interaction of the electron system, light, and phonons. The electron-radiation interaction is given by the $\boldsymbol{A}\cdot\boldsymbol{p}$ term in the expansion of the Hamiltonian of an electron in the presence of a field characterized by a vector potential $\boldsymbol{A}$ [21]. Using a second-quantization formalism and assuming an incident photon of angular frequency ω and polarization μ, we

can write this term as

$$H_{eR} = \frac{M_R}{\sqrt{V}} \sum_{\boldsymbol{k},\sigma,\nu} (\hat{\mathbf{e}}_\mu \cdot \boldsymbol{P}_{\sigma\boldsymbol{k},\nu\boldsymbol{k}}) c^\dagger_{\sigma\boldsymbol{k}} v_{\nu\boldsymbol{k}} (a^\dagger_\mu + a_\mu);$$

$$M_R = \left(\frac{e}{m}\right)\left(\frac{4\pi}{n^2_{op}}\right)^{1/2}\left(\frac{\hbar}{2\omega}\right)^{1/2}. \tag{3}$$

Here $c^\dagger_{\sigma\boldsymbol{k}}(c_{\sigma\boldsymbol{k}})$ is the creation (annihilation) operator for a conduction band electron with wave vector k and spin σ; $v^\dagger_{\nu\boldsymbol{k}}(v_{\nu\boldsymbol{k}})$ the creation (annihilation) operator for a valence band electron with wave vector k in band $\nu = 1, 2, 3, 4$, as in Eq. (2); and $a^\dagger_\mu(a_\mu)$ is the creation (annihilation) operator for the photon. This Hamiltonian can only induce vertical transitions between bands because we are neglecting the photon wave vector, a standard approximation at optical frequencies. The electron-light coupling is characterized by a momentum matrix element $\hat{\mathbf{e}}_\mu \cdot \boldsymbol{P}_{\sigma\boldsymbol{k},\nu\boldsymbol{k}}$ where $\hat{\mathbf{e}}_\mu$ is a unit light polarization vector. In the prefactor M_R, n_{op} is the material's index of refraction at frequency ω; e is free electron charge; m the free electron mass; and $\hbar$ the reduced Planck's constant. The normalization volume V is taken as the macroscopic sample volume.

For states near the Γ point of the BZ, the momentum matrix elements can be written in terms of the $\boldsymbol{k}\cdot\boldsymbol{p}$-theory parameter P, defined as [20]

$$\begin{aligned} P &= -i\langle S\uparrow|P_x|X\uparrow\rangle = -i\langle S\uparrow|P_y|Y\uparrow\rangle \\ &= -i\langle S\uparrow|P_z|Z\uparrow\rangle = -i\langle S\downarrow|P_x|X\downarrow\rangle \\ &= -i\langle S\downarrow|P_y|Y\downarrow\rangle = -i\langle S\downarrow|P_z|Z\downarrow\rangle. \end{aligned} \tag{4}$$

With this definition, the effective mass of electrons in the Γ valley, $m_{e\Gamma}$, is given by

$$\frac{1}{m_{e\Gamma}} = \frac{1}{m} + \frac{2}{3}\left(\frac{P}{m}\right)^2\left[\frac{2}{E_0} + \frac{1}{E_0 + \Delta_0}\right], \tag{5}$$

where m is the free electron mass. For the momentum matrix elements $\hat{\mathbf{e}}_\mu \cdot \boldsymbol{P}_{\sigma\boldsymbol{k},\nu\boldsymbol{k}}$ we neglect, as usual, their dependence on the wave-vector magnitude k, but we must consider the relative orientation between $\boldsymbol{k}$ and the polarization vector $\mathbf{e}_\mu$. However, since we eventually perform integrations over $\boldsymbol{k}$, we can use angular averages $P_{\sigma\nu}$ such that $P^2_{\sigma\nu} = \lim_{k\to 0} \overline{|\mathbf{e}_\mu \cdot \boldsymbol{P}_{\boldsymbol{k},\sigma;\boldsymbol{k},\nu}|^2}$, as discussed in Ref. [22]. We then obtain

$$\begin{aligned} P^2_{\uparrow 1} &= P^2_{\downarrow 3} = \frac{P^2}{3}, \\ P^2_{\uparrow 2} &= P^2_{\downarrow 4} = \frac{2P^2}{9}, \\ P^2_{\uparrow 4} &= P^2_{\downarrow 2} = \frac{P^2}{9}, \end{aligned} \tag{6}$$

all other couplings being zero. Using these angular averages in Eq. (3), the electron-radiation coupling is characterized by a single parameter P.

Since H_{eR} can only effect vertical transitions, absorption across the indirect gap requires the additional momentum provided by a phonon. The electron-phonon Hamiltonian relevant for resonant indirect absorption couples the conduction band states at Γ and L via LA phonons [15]. The corresponding Hamiltonian [23,24] is given in second-quantization notation by

$$H_{eP} = \frac{M_P D_{\Gamma L}}{\sqrt{V}} \sum_{\boldsymbol{k}\boldsymbol{q}\sigma} c^+_{\sigma\boldsymbol{k}} c_{\sigma,\boldsymbol{k}-\boldsymbol{q}} [b_{\boldsymbol{q},\mathrm{LA}} - b^\dagger_{-\boldsymbol{q},\mathrm{LA}}];$$

$$M_P = \sqrt{\frac{\hbar}{2\rho\Omega_{\mathrm{LA}}}}, \tag{7}$$

where ρ is the material's density, Ω_{LA} is the LA phonon angular frequency, and $D_{\Gamma L}$ is the so-called deformation potential (with units of energy/distance). In this expression we are neglecting the wave-vector dependence of the deformation potential and phonon frequency, so that their values should be viewed as an average. This makes it possible to characterize the electron-phonon interaction with a single parameter, similarly to our approximations for the electron-radiation Hamiltonian.

As we will see later, the value of $D_{\Gamma L}$ is critical for the assessment of any theory of indirect optical absorption. From time-resolved transmission experiments, Zhou *et al.* [25] find $D_{\Gamma L} = (4.2 \pm 0.2) \times 10^8$ eV/cm. By studying the pressure dependence of the direct gap exciton at low temperature, Li and co-workers [26] obtained an upper limit $D_{\Gamma L} < 4.5 \times 10^8$ eV/cm, which is consistent with Zhou's measurements. Theoretical predictions are in good agreement with the experimental data. Krishnamurthy and Cardona [27] find $D_{\Gamma L} = 3.9 \times 10^8$ eV/cm using an *ab initio* tight-binding method and a frozen-phonon calculation. From electronic structure calculations within the local-density approximation (LDA) to density-functional theory, combined with density-functional perturbation theory for phonons, Tyuterev *et al.* obtained $D_{\Gamma L} = 4.0 \times 10^8$ eV/cm [28]. Using instead a frozen-phonon approach, Murphy-Armando and Fahy [29] found $D_{\Gamma L} = 4.1 \times 10^8$ eV/cm. In our fits of experimental data to be discussed below, $D_{\Gamma L}$ will be taken as an adjustable parameter, and the agreement with these well-established values will be an important criterion to decide on the absorption model validity. The remaining Ge parameters will not be adjusted but taken from the literature [23,25,30–36]. They are summarized in Table I. Some of these parameters were computed from available data at low temperature as described in Appendix B.

Using Eqs. (3) and (7), optical absorption can be calculated as an exercise in second-order perturbation theory. For this, we note that intermediate as well as final states contain one electron in the conduction band and one hole in the valence band, so it is convenient to introduce an excitonic representation by defining the operators [37]:

$$d^\dagger_{\lambda\boldsymbol{K},\sigma\nu} = \frac{1}{\sqrt{N}} \sum_{\boldsymbol{R}\boldsymbol{k}} U_{\lambda\boldsymbol{K},\sigma\nu}(\boldsymbol{R}) e^{-i\boldsymbol{k}\cdot\boldsymbol{R}} c^\dagger_{\sigma\boldsymbol{k}} v_{\nu,\boldsymbol{k}-\boldsymbol{K}}. \tag{8}$$

Here N is the number of unit cells in the crystal, $\boldsymbol{K}$ is the electron-hole pair's (exciton's) center of mass wave vector, and λ is an index that represents the internal degrees of freedom of the exciton. The indices σ and ν [from Eqs. (1) and (2)] identify the conduction and valence bands involved, and $\boldsymbol{R}$ is a relative lattice vector that represents the electron-hole separation. The function $U_{\lambda\boldsymbol{K},\sigma\nu}(\boldsymbol{R})$ depends on the electron-hole interaction. For Wannier-like excitons with large electron-hole separations, the variable $\boldsymbol{R}$ can be taken as continuous, and one

TABLE I. Material parameters at the experimental temperature of 301 K used for the calculation of the absorption coefficient of Ge. The columns that lack a direct reference were computed from available experimental data as discussed in Appendix B. In the case of $n_{\rm op}$ and ε_0, they were taken from our own ellipsometric measurements.

$m_{e\Gamma}/m$	$m_\perp/m$	$m_{\|\|}/m$	m_{lh}/m	m_{hh}/m	P^2/m (eV)	$\hbar\Omega_{\rm LA}$ (meV)	$\hbar\Omega_{\rm O}$ (meV)	ρ (g/cm^3)	$D_{\Gamma L}$(eV/cm)	d_0(eV)	$n_{\rm op}$	ε_0	a_0(Å)
0.0338	0.0784	1.58[a–c]	0.0385	0.352	12.61	27[d]	37.2[e]	5.323[f]	4.2×10^8[g]	41[h]	4.13	16.2	5.6574

[a]Reference [30]; [b]Reference [31]; [c]Reference [32]; [d]Reference [33]; [e]Reference [35]; [f]Reference [36]; [g]Reference [25]; [h]Reference [34].

can obtain $U_{\lambda\boldsymbol{K},\sigma\nu}(\boldsymbol{R})$ from the solution of Schrödinger-like differential equations.

For the purpose of calculating resonant indirect absorption we need to consider two types of exciton. When both the electron and hole states are near the Γ point of the BZ, we define a function $F_{\lambda\boldsymbol{K},\sigma\nu}(\boldsymbol{R}) = v_c^{-1/2} e^{-is_{e\Gamma\nu}\boldsymbol{K}\cdot\boldsymbol{R}} U_{\lambda\boldsymbol{K},\sigma\nu}(\boldsymbol{R})$, where v_c is the volume of the unit cell, and $s_{e\Gamma\nu} = m_{e\Gamma}/M_{\Gamma\nu}$, with $M_{\Gamma\nu} = m_{e\Gamma} + m_\nu$. In the limit in which $\boldsymbol{R}$ can be taken as a continuum variable, $F_{\lambda\boldsymbol{K},\sigma\nu}(\boldsymbol{R})$ satisfies a hydrogenic Schrödinger equation with bound eigenvalues, $E_{\lambda K\nu} \equiv E_{nK\nu} = E_0 + \hbar^2K^2/2M_{\Gamma\nu} - R_{y\Gamma\nu}/n^2$, $n = 1, 2, 3\cdots$. Here the excitonic Rydberg is $R_{y\Gamma\nu} = \mu_{\Gamma\nu}e^4/2\hbar^2\varepsilon_0^2$, where $\mu_{\Gamma\nu}^{-1} = m_{e\Gamma}^{-1} + m_\nu^{-1}$, and ε_0 is the static dielectric constant. The second type of exciton we will consider involves the same hole states as the previous one but electrons near the L-point minimum of the CB. Since the conduction band effective mass is very anisotropic at this point, the resulting Schrödinger-like equation does not have simple analytical solutions. We will therefore follow Elliott and make the drastic approximation that the band dispersion is spherically symmetric around L: $E_c(\boldsymbol{k}) = E_{\rm ind} + \hbar^2(\boldsymbol{k}-\boldsymbol{k}_L)/2m_L$ with $k_L = \frac{\pi}{a_0}(1,1,1)$ with a_0 being the cubic lattice parameter. The validity of this spherical approximation will be discussed below. Under this assumption we recover a hydrogenlike Schrödinger exciton equation for $F_{\lambda\boldsymbol{K},\sigma\nu}(\boldsymbol{R}) = v_c^{-1/2} e^{-i(s_{eL\nu}\boldsymbol{K}+s_{hL\nu}\boldsymbol{k}_L)\cdot\boldsymbol{R}} U_{\lambda\boldsymbol{K},\sigma\nu}(\boldsymbol{R})$, where $s_{eL\nu} = m_L/M_{L\nu}$, $s_{hL\nu} = m_\nu/M_{L\nu}$, and $M_{L\nu} = m_L + m_\nu$. The corresponding bound eigenvalues are given by $E_{\lambda K\nu} \equiv E_{nK\nu} = E_{\rm ind} + \hbar^2(\boldsymbol{K}-\boldsymbol{k}_L)^2/2M_{L\nu} - R_{yL\nu}/n^2$, $n = 1, 2, 3\cdots$ with $R_{yL\nu} = \mu_{L\nu}e^4/2\hbar^2\varepsilon_0^2$ and $\mu_{L\nu}^{-1} = m_L^{-1} + m_\nu^{-1}$.

Notice that our description of the excitons assumes separate excitonic states for each valence band involved. This is, strictly speaking, never the case, since light and heavy holes are degenerate at the Γ point. However, within the spherical approximations to be discussed in Sec. II C, the problem does reduce to the sum of two separate two-band excitonic contributions, albeit with excitons calculated using different effective masses. The expressions derived next contain a sum over the two types of hole, which in Sec. II C will be replaced by a factor of 2 times the contribution of a "hybrid" light-/heavy-hole state.

The intensity of radiation traveling a distance dx in a medium is attenuated as $dI/I = -\alpha dx$, where α is the absorption coefficient. If the transition rate for the process is $R_{i\to f}$, then $\alpha = R_{i\to f}n_{op}/c$, where c is the speed of light in vacuum. For typical experimental conditions $k_BT \ll E_{\rm ind}$, where k_B is Boltzmann's constant. In this limit it is an excellent approximation to assume that the initial state $|i\rangle$ consists of an electronic system in its ground state, a phonon bath, and an incident photon with fixed polarization μ. We indicate this initial state as $a_\mu^\dagger|G\rangle$. The final state $|f\rangle$ consists of an exciton and one additional (creation) or one less (annihilation) phonon. It is given in bra form as $[n_{\boldsymbol{q}\rm LA}+1]^{-1/2}\langle G|b_{\boldsymbol{q}\rm LA}d_{\lambda\boldsymbol{K},\sigma\nu}$ or $(n_{\boldsymbol{q}\rm LA})^{-1/2}\langle G|b_{\boldsymbol{q}\rm LA}^\dagger d_{\lambda\boldsymbol{K},\sigma\nu}$, respectively, where the prefactors containing the Bose-Einstein phonon population $n_{\boldsymbol{q}_{\rm LA}}$ insure proper normalization. The intermediate states consist of excitons of the form $d_{\lambda\boldsymbol{K},\sigma\nu}^\dagger|G\rangle$. Therefore, the dominant contributions to the transition rate are, from Fermi's "golden rule,"

$$R_{i\to f}^{\pm} = \frac{2\pi}{\hbar}\sum_{\boldsymbol{q},\lambda\boldsymbol{K},\sigma\nu}\left|\left(n_{\boldsymbol{q}\rm LA}+\frac{1}{2}\pm\frac{1}{2}\right)^{-1/2}\sum_{\lambda'\boldsymbol{K}',\sigma'\nu'}\frac{\langle G|b_{\boldsymbol{q}\rm LA}d_{\lambda\boldsymbol{K},\sigma\nu}H_{eL}d_{\lambda'\boldsymbol{K}',\sigma'\nu'}^\dagger|G\rangle\langle G|d_{\lambda'\boldsymbol{K}',\sigma'\nu'}H_{eR}a_\mu^\dagger|G\rangle}{\hbar\omega - E_{\lambda'\boldsymbol{K}',\sigma'\nu'}}\right|^2 \times\delta(E_{\lambda\boldsymbol{K},\sigma\nu}\pm\hbar\Omega_{\rm LA}-\hbar\omega). \tag{9}$$

Here the upper "+" sign corresponds to phonon creation and the lower "−" sign to phonon annihilation. Equation (9) omits a contribution from terms in which H_{eL} and H_{eR} appear in reverse order. These are zero under our assumptions that the electronic system is initially in its ground state and that H_{eL} does not couple the valence band with the conduction band.

The matrix elements in Eq. (9) can be easily computed from the definitions in Eqs. (3), (7), and (8), combined with well-known theorems for lattice sums. First we observe that if the final state contains a conduction band (CB) electron at the L point, this state can be reached via a direct optical transition at Γ followed by an electron-phonon "transfer" of the electron from Γ to L, as shown in Fig. 1 as processes 1 and 2. Alternatively, it is possible to have a direct optical transition at L (across the so-called E_1 and $E_1+\Delta_1$ gaps) followed by an electron-phonon "transfer" of the hole from L to Γ. This is indicated as processes $1'$ and $2'$ in Fig. 1. However, the first process, with intermediate energies $E_{\lambda'\boldsymbol{K}',\sigma'\nu'} \sim 0.8$ eV, is far more resonant than the latter, with $E_{\lambda'\boldsymbol{K}',\sigma'\nu'} \sim 2$ eV. Accordingly, we will neglect the contribution from the E_1 and $E_1+\Delta_1$ transitions. In this case, the exciton created by the H_{eR} element is a Γ-point exciton, whereas H_{eL} converts this

Γ-point exciton into an indirect exciton with the electron near L and the hole near Γ. The matrix elements become

$$\langle G|d_{\lambda' \boldsymbol{K}',\sigma'\nu'} H_{eR} a^\dagger_\mu|G\rangle = \delta_{\boldsymbol{K}',\boldsymbol{0}} M_R P_{\sigma'\nu'} F^*_{\lambda'\boldsymbol{0},\sigma'\nu'}(\boldsymbol{0}), \tag{10}$$

and

$$\langle G|b_{\boldsymbol{q}\mathrm{LA}} d_{\lambda \boldsymbol{K},\sigma\nu} H_{eL} d^\dagger_{\lambda'\boldsymbol{0},\sigma'\nu'}|G\rangle = -\frac{M_P D_{\Gamma L}}{\sqrt{V}} v_c[n_{\mathrm{LA}}+1]\delta_{\nu\nu'}\delta_{\sigma\sigma'}\delta_{-\boldsymbol{q},\boldsymbol{K}} \sum_{\boldsymbol{R}} F^*_{\lambda\boldsymbol{K},\sigma\nu}(\boldsymbol{R}) F_{\lambda\boldsymbol{0},\sigma\nu}(\boldsymbol{R}) e^{i s_{hL\nu}(\boldsymbol{K}-\boldsymbol{k}_L)\cdot\boldsymbol{R}},$$

$$\langle G|b^\dagger_{\boldsymbol{q}\mathrm{LA}} d_{\lambda \boldsymbol{K},\sigma\nu} H_{eL} d^\dagger_{\lambda'\boldsymbol{0},\sigma'\nu'}|G\rangle = \frac{M_L D_{\Gamma L}}{\sqrt{V}} v_c[n_{\mathrm{LA}}]\delta_{\nu\nu'}\delta_{\sigma\sigma'}\delta_{\boldsymbol{q},\boldsymbol{K}} \sum_{\boldsymbol{R}} F^*_{\lambda\boldsymbol{K},\sigma\nu}(\boldsymbol{R}) F_{\lambda\boldsymbol{0},\sigma\nu}(\boldsymbol{R}) e^{i s_{hL\nu}(\boldsymbol{K}-\boldsymbol{k}_L)\cdot\boldsymbol{R}}. \tag{11}$$

Inserting (10) and (11) into Eq. (9), we obtain

$$R^{\pm}_{i\to f} = \frac{2\pi}{\hbar}\frac{M_P^2 M_R^2}{V} D^2_{\Gamma L} v_c^2 \left[n_{\mathrm{LA}} + \frac{1}{2} \pm \frac{1}{2}\right] \sum_{\lambda\boldsymbol{K},\sigma\nu} |P_{\sigma\nu}|^2 \left| \sum_{\boldsymbol{R}} F^*_{\lambda\boldsymbol{K},\sigma\nu}(\boldsymbol{R}) e^{i s_{hL\nu}(\boldsymbol{K}-\boldsymbol{k}_L)\cdot\boldsymbol{R}} \sum_{\lambda'} \frac{F_{\lambda'\boldsymbol{0},\sigma\nu}(\boldsymbol{R}) F^*_{\lambda'\boldsymbol{0},\sigma\nu}(\boldsymbol{0})}{\hbar\omega - E_{\lambda'\boldsymbol{0},\sigma\nu}} \right|^2$$
$$\times \delta(E_{\lambda\boldsymbol{K},\sigma\nu} \pm \hbar\Omega_{\mathrm{LA}} - \hbar\omega). \tag{12}$$

Upon substitution of the expressions for the momentum matrix elements in Eq. (6), we obtain:

$$R^{\pm}_{i\to f} = \frac{2\pi}{\hbar}\frac{M_P^2 M_R^2}{V} \left(\frac{2P^2}{3}\right) D^2_{\Gamma L} v_c^2 [n_{\mathrm{LA}}+1] \sum_{\lambda\boldsymbol{K}h} \left| \sum_{\boldsymbol{R}} F^*_{\lambda\boldsymbol{K},h}(\boldsymbol{R}) e^{i s_{hL}(\boldsymbol{K}-\boldsymbol{k}_L)\cdot\boldsymbol{R}} \sum_{\lambda'} \frac{F_{\lambda'\boldsymbol{0},h}(\boldsymbol{R}) F^*_{\lambda'\boldsymbol{0},h}(\boldsymbol{0})}{\hbar\omega - E_{\lambda'\boldsymbol{0},h}} \right|^2$$
$$\times \delta(E_{\lambda\boldsymbol{K},h} \pm \hbar\Omega_{\mathrm{LA}} - \hbar\omega), \tag{13}$$

where the index h now runs over light and heavy holes. Since all sums over the index ν are "collapsed" into a sum over the two types of holes, we will from now replace the subscript "ν" in all previously defined symbols with "h," except that s_{hLh} and $s_{h\Gamma h}$ are simplified as s_{hL} and $s_{h\Gamma}$.

Equation (13) transparently displays the alternative physics required to describe indirect excitons in Ge. If the energy denominator $\hbar\omega - E_{\lambda'\boldsymbol{0},h}$ is independent of λ', i.e., if all intermediate states are assumed to have the same energy, we are left with the completeness relation $\sum_{\lambda'} F_{\lambda'\boldsymbol{0},h}(\boldsymbol{R}) F^*_{\lambda'\boldsymbol{0},h}(\boldsymbol{0}) = \delta(\boldsymbol{R})$, and the transition rate becomes proportional to $|F_{\lambda\boldsymbol{K},h}(\boldsymbol{0})|^2$. This is the result obtained by Elliott [14]. It is similar to the expression for direct excitonic absorption in that it depends on the final state excitonic wave function at position $\boldsymbol{R} = \boldsymbol{0}$. Furthermore, since the completeness relation is independent of the strength of the electron-hole interaction, the final result is identical whether we treat the intermediate states as free electron-hole pairs or as excitons. In the case of Ge, however, the approximation of extracting the denominator from the sum over λ' is very poor. This implies that in a realistic theory the nature of the intermediate states will affect the transition rate. Furthermore, the transition rate will depend not only on the final state excitonic wave function at $\boldsymbol{R} = \boldsymbol{0}$ but at all values of $\boldsymbol{R}$. It is therefore inconsistent to calculate the indirect absorption using the Hartman model and then attempt to correct for excitonic effects using the Elliott approximations.

B. Green's function theory

The computation of Eq. (13) is greatly facilitated by noting that

$$G^h_{\hbar\omega}(\boldsymbol{R},\boldsymbol{0}) = \sum_{\lambda} \frac{F^*_{\lambda\boldsymbol{0},h}(\boldsymbol{0}) F_{\lambda\boldsymbol{0},h}(\boldsymbol{R})}{\hbar\omega - E_{\lambda\boldsymbol{0},h}} \tag{14}$$

is the Green's function for the excitonic Schrödinger equation [38]. For the Γ-point excitons relevant to our calculation this Green's function has a particularly simple form [39–41] in the limit in which $\boldsymbol{R}$ can be considered a continuum variable. In this case the Green's function depends only on the magnitude $R \equiv |\boldsymbol{R}|$ according to

$$G^h_{\hbar\omega}(\boldsymbol{R},\boldsymbol{0}) = \left(\frac{1}{4\pi R}\right)\left(\frac{2\mu_{\Gamma h}}{\hbar^2}\right)\Gamma(1-\kappa_{\Gamma h}) W_{\kappa_{\Gamma h},1/2}(\rho), \tag{15}$$

with

$$\kappa_{\Gamma h} = \sqrt{\left(\frac{R_{y\Gamma h}}{E_0 - \hbar\omega}\right)}; \quad \mathrm{Re}\kappa_{\Gamma h} \geqslant 0, \mathrm{Im}\kappa_{\Gamma h} \geqslant 0,$$
$$\rho = \frac{2R}{\kappa a_{B\Gamma h}}; \quad a_{B\Gamma h} = \frac{\hbar}{\sqrt{2\mu_{\Gamma h} R_{y\Gamma h}}}. \tag{16}$$

Here $\Gamma(z)$ is the Gamma function (not to be confused with the Γ point in the BZ), and $W_{\kappa,n}(z)$ a Whittaker function of the first kind.

Using the Green's function, and converting the sum over $\boldsymbol{R}$ in Eq. (13) into an integral, we obtain

$$R^{\pm}_{i\to f} = \frac{2\pi}{\hbar}\frac{M_P^2 M_R^2}{V} \left(\frac{2P^2}{3}\right) D^2_{\Gamma L} \left[n_{\mathrm{LA}} + \frac{1}{2} \pm \frac{1}{2}\right]$$
$$\times \sum_{\lambda\boldsymbol{K}h} \left| \int_V d\boldsymbol{R} F^*_{\lambda\boldsymbol{K},h}(\boldsymbol{R}) e^{i s_{hL}(\boldsymbol{K}-\boldsymbol{k}_L)\cdot\boldsymbol{R}} G^h_{\hbar\omega}(R,\boldsymbol{0}) \right|^2$$
$$\times \delta(E_{\lambda\boldsymbol{K},h} \pm \hbar\Omega_{\mathrm{LA}} - \hbar\omega). \tag{17}$$

To evaluate this transition rate we need the final state excitonic wave function $F_{\lambda\boldsymbol{K},h}(\boldsymbol{R})$. For bound states, the generic index λ can be identified with the hydrogenic quantum numbers n, l, m. In the Elliott exciton limit the absorption is proportional to $|F_{\lambda\boldsymbol{K},h}(\boldsymbol{0})|^2$, as discussed above, which is

nonzero only for the s-like $l = 0$ excitons. While this is not the case in Eq. (17), the contribution from the $l \neq 0$ states will be necessarily small because each excitonic state contributes a term roughly proportional to n^{-3}. Accordingly, the contribution from the $2p$ state will not exceed 10% and will probably be even less, since it vanishes in the limit of constant denominators. Furthermore, we will find below that the excitonic continuum states make a much larger contribution to the absorption, so that we will neglect any $l \neq 0$ bound state. Under this approximation $F_{\lambda \boldsymbol{K},h}(\boldsymbol{R})$ depends only on the magnitude R and the principal quantum number n according to

$$F_{\lambda \boldsymbol{K},h}(\boldsymbol{R}) \equiv F_{n\boldsymbol{K},h}(R) = \frac{1}{\sqrt{\pi}(n a_{BLh})^{3/2}} \frac{1}{n} e^{-\rho/2} L^1_{n-1}(\rho);$$
$$\rho = \frac{2R}{\kappa_{Lh} a_{BLh}}; \quad a_{BLh} = \frac{\hbar}{\sqrt{2\mu_{Lh} R_{yLh}}}, \tag{18}$$

where $L^1_n(\rho)$ is an associated Laguerre polynomial of order n. Here, in analogy with Eq. (16),

$$\kappa_{Lh} = \sqrt{\left(\frac{R_{yLh}}{E_0 - \hbar\omega}\right)}; \quad \mathrm{Re}\kappa_{Lh} \geqslant 0, \mathrm{Im}\kappa_{Lh} \geqslant 0,$$
$$\rho = \frac{2R}{\kappa a_{BLh}}; \quad a_{BLh} = \frac{\hbar}{\sqrt{2\mu_{Lh} R_{yLh}}}. \tag{19}$$

For the continuum limit the index λ becomes a wave vector $\boldsymbol{k}$, and the corresponding energy is $E_{\boldsymbol{k}\boldsymbol{K}h} \equiv E_{n\boldsymbol{K}\nu} = E_{\mathrm{ind}} + \hbar^2(\boldsymbol{K} - \boldsymbol{k}_L)^2/2M_{Lh} + \hbar^2 k^2/2\mu_{Lh}$, with $k = |\boldsymbol{k}|$. The wave function can be written as [42]

$$F_{\lambda \boldsymbol{K},h}(\boldsymbol{R}) \equiv F_{\boldsymbol{k}\boldsymbol{K},h}(\boldsymbol{R})$$
$$= \frac{1}{\sqrt{V}} \Gamma(1 + i\nu_{Lh}) e^{\pi \nu_{Lh}/2}$$
$$\times e^{i\boldsymbol{k}\cdot\boldsymbol{R}} {}_1F_1(-i\nu_{Lh}, 1, -ikR - i\boldsymbol{k}\cdot\boldsymbol{R}), \tag{20}$$

with

$$\nu_{Lh} = \sqrt{\frac{R_{yLh}}{\hbar^2 k^2/2\mu_{Lh}}}. \tag{21}$$

Here ${}_1F_1(a, b, z)$ is a confluent hypergeometric function of the first kind. It is interesting to point out that Elliott [14] writes his final state wave function as a partial wave expansion into spherical harmonics (see Eq. 2.10 in Ref. [14]). Such a form is convenient given the $l = 0$ selection rule of the Elliott model, but Eq. (20) is far more compact for our purposes. Furthermore, in the limit of vanishing Coulomb interaction, $\nu_{Lh} \to 0$, and Eq. (20) reduces to a plane wave, which makes it very simple to compute the nonexcitonic absorption limit.

1. Bound exciton calculation

Even after the considerable simplifications discussed above, the transition rate in Eq. (17) cannot be computed analytically. For bound excitons, however, our approximated final state wave function as well as the Green's function that appears in the integral over R is spherically symmetric. This makes it possible to carry out the angular part of the integration analytically by placing the vector $\boldsymbol{K} - \boldsymbol{k}_L$ along the z axis. We then find

$$R^{\pm}_{i\to f} = \frac{2\pi}{\hbar} \frac{M_P^2 M_R^2}{V} \left(\frac{2P^2}{3}\right) D^2_{\Gamma L} \left[n_{\mathrm{LA}} + \frac{1}{2} \pm \frac{1}{2}\right]$$
$$\times \sum_{n\boldsymbol{K}h} \frac{1}{n^5} |H_{Lnh}(|\boldsymbol{K} - \boldsymbol{k}_L|)|^2$$
$$\times \delta\left[E_{\mathrm{ind}} + \frac{\hbar^2(\boldsymbol{K} - \boldsymbol{k}_L)^2}{2M_{Lh}} - \frac{R_{yLh}}{n^2} \pm \hbar\Omega_{\mathrm{LA}} - \hbar\omega\right], \tag{22}$$

where

$$H_{Lnh}(k) = \frac{R_{yLh}}{s_{hL} k} \int_0^\infty dR R \sin(s_{hL} k R) G^h_{\hbar\omega}(R, 0)$$
$$\times e^{-\frac{R}{n a_{BLh}}} L^1_{n-1}\left(\frac{2R}{n a_{BLh}}\right). \tag{23}$$

Performing a change of variables $\boldsymbol{k}' = \boldsymbol{K} - \boldsymbol{k}_L$ and converting the sum over $\boldsymbol{k}'$ into an integral over the variable $\varepsilon' = \hbar^2 k'^2/2M_{Lh}$, we finally obtain, after some straightforward manipulations,

$$\alpha^{\pm}_{\mathrm{bound}}$$
$$= \frac{512 n_{op}}{3\hbar^7 c} M_R^2 M_P^2 P^2 D^2_{\Gamma L} \left(n_{\mathrm{LA}} + \frac{1}{2} \pm \frac{1}{2}\right)$$
$$\times \sum_h \sum_n (m_L m_h)^{3/2} \frac{R_{yLh}^{-1/2}}{n^5}$$
$$\times \left(\hbar\omega - E_{\mathrm{ind}} + \frac{R_{yLh}}{n^2} \mp \hbar\Omega_{\mathrm{LA}}\right)^{1/2}$$
$$\times \left| H_{Lhn}\left[\frac{\sqrt{2M_{Lh}}}{\hbar}\left(\hbar\omega - E_{\mathrm{ind}} + \frac{R_{yLh}}{n^2} \mp \hbar\Omega_{\mathrm{LA}}\right)^{1/2}\right]\right|^2, \tag{24}$$

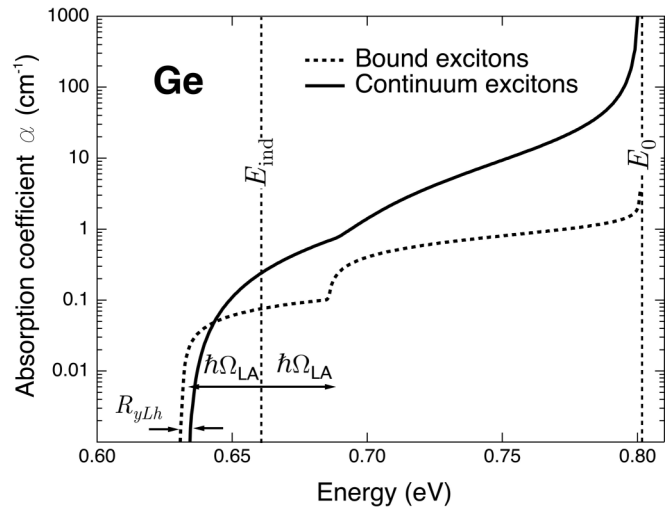

FIG. 2. Calculated absorption coefficient of Ge using parameters from Table I. The dotted line shows the bound exciton contribution, from Eq. (24), and the solid line corresponds to the continuum exciton contribution, Eq. (29). In both cases we use effective masses from Eq. (47).

where we have multiplied the expression obtained from Eq. (22) by a factor of $8/2 = 4$ to take into account the valley degeneracy along the different $\langle 111 \rangle$ directions in Ge. We have also used the identity $M_{Lh}\mu_{Lh} = m_L m_h$. The function H_{Lhn} is computed by numerical integration. The calculated absorption coefficient from Eq. (24) is shown in Fig. 2. Notice the well-known result that bound excitons contribute to the absorption above and below the indirect band gap. This is in contrast with the direct gap absorption case, in which bound excitons only contribute to below-band-gap absorption. Therefore, we must take bound exciton absorption into account, even though our primary focus is on the more resonant energy range between the indirect and direct gaps. However, as seen in Fig. 2 and derived below, the continuum exciton absorption is one order of magnitude stronger in this range.

2. Continuum exciton calculation

For the continuum case, the presence of the argument $\boldsymbol{k}\cdot\boldsymbol{R}$ in Eq. (20) means that the integral over $\boldsymbol{R}$ in Eq. (17) involves a nontrivial angular integration. In addition, the final result of this $\boldsymbol{R}$ integration depends on the relative angle between $\boldsymbol{k}$ and $\boldsymbol{K}$, which implies that the complete evaluation of Eq. (17) requires a quadruple integral at each photon energy. This is computationally too costly if we want to run the calculations on personal computers and eventually fit experimental data. The calculation can be made more manageable if we introduce the approximation

$$ {}_1F_1(-i\nu, 1, -ikR - i\boldsymbol{k}\cdot\boldsymbol{R}) \simeq {}_1F_1(-i\nu, 1, -ikR). \quad (25)$$

This approximation will be justified below. Qualitatively, this simplification is consistent with our neglect of mass anisotropy in the underlying Schrödinger equation. Inserting Eq. (25) into (17), and using again the change of variable $\boldsymbol{k}' = \boldsymbol{K} - \boldsymbol{k}_L$, we obtain

$$R^{\pm}_{i\to f} = \frac{2\pi}{\hbar}\frac{M_P^2 M_R^2}{V^2}\left(\frac{2P^2}{3}\right)D_{\Gamma L}^2\left[n_{\rm LA}+\frac{1}{2}\pm\frac{1}{2}\right]\sum_{\boldsymbol{k}\boldsymbol{k}'h}\left|\Gamma(1+i\nu_{Lh})e^{\pi\nu_{Lh}/2}\int_V d\boldsymbol{R}\,{}_1F_1^*(-i\nu,1,-ikR)e^{i\boldsymbol{k}_h\cdot\boldsymbol{R}}G^h_{\hbar\omega}(R,0)\right|^2$$
$$\times\,\delta\left(E_{\rm ind}+\frac{\hbar^2k'^2}{2M_{Lh}}+\frac{\hbar^2k^2}{2\mu_{Lh}}\pm\hbar\Omega_{\rm LA}-\hbar\omega\right), \quad (26)$$

with $\boldsymbol{k}_h = s_{hL}(\boldsymbol{K}-\boldsymbol{k}_L)-\boldsymbol{k} = s_{hL}\boldsymbol{k}'-\boldsymbol{k}$. If the integral over $\boldsymbol{R}$ is carried out in spherical coordinates, the angular integrations can be done analytically, and we obtain

$$R^{\pm}_{i\to f} = \frac{8\pi}{\hbar}\frac{M_P^2 M_R^2}{V^2}\left(\frac{2P^2}{3}\right)D_{\Gamma L}^2\left[n_{\rm LA}+\frac{1}{2}\pm\frac{1}{2}\right]\left(\frac{4\pi}{R_{yLh}}\right)^2\sum_{\boldsymbol{k}\boldsymbol{k}'h}|J_{Lh}(k,k',\theta)|^2\,\delta\left(E_{\rm ind}+\frac{\hbar^2k'^2}{2M_{Lh}}+\frac{\hbar^2k^2}{2\mu_{Lh}}\pm\hbar\Omega_{\rm LA}-\hbar\omega\right), \quad (27)$$

where we have again multiplied the expression by a factor of 4 to account for valley degeneracy. The function $J_{Lh}(k,k',\theta)$ is defined as

$$J_{Lh}(k,k',\theta) = \frac{R_{yLh}\Gamma(1+i\nu_{Lh})e^{\pi\nu_{Lh}/2}}{k_h}\int_0^\infty dR\,R\,G_{\hbar\omega}(R,0)\,{}_1F_1^*(-i\nu_{Lh},1,-ikR)\sin k_h R, \quad (28)$$

where θ is the angle between $\boldsymbol{k}$ and $\boldsymbol{k}'$ such that $k_h^2 = s_{hL}^2k'^2 + k^2 - 2s_{hL}kk'\cos\theta$. Next we convert the sums over $\boldsymbol{k}$ and $\boldsymbol{k}'$ into integrals and introduce the variables $\varepsilon = \hbar^2k^2/2\mu_{Lh}$ and $\varepsilon' = \hbar^2k'^2/2M_{Lh}$, so that we finally obtain

$$\alpha^{\pm}_{\rm continuum} = \frac{64n_{op}}{3\hbar^7\pi c}M_P^2M_R^2P^2D_{\Gamma L}^2\left[n_{\rm LA}+\frac{1}{2}\pm\frac{1}{2}\right]\sum_h\left(\frac{1}{R_{yLh}}\right)^2 m_L^{3/2}m_h^{3/2}\int_0^\pi d\theta\,\sin\theta$$
$$\times\int_0^{\hbar\omega\mp\hbar\Omega_{\rm LA}} d\varepsilon\,|J[k(\varepsilon),k'(\hbar\omega-\varepsilon\mp\hbar\Omega_{\rm LA}),\theta]|^2\sqrt{\hbar\omega-\varepsilon\mp\hbar\Omega_{\rm LA}}\sqrt{\varepsilon}. \quad (29)$$

Equation (29) is evaluated numerically as a triple integral over the position R, the angle θ, and the energy ε.

3. Free electron-hole pair limit

In the limit of vanishing electron-hole interaction, $\kappa_{\Gamma h}\to 0$ in Eq. (16), and since $W_{0,1/2}(\rho) = e^{-\rho/2}$ and $\Gamma(1) = 1$, we obtain

$$\lim_{\kappa_{\Gamma h}\to 0} G^h_{\hbar\omega}(R,0) = \left(\frac{1}{4\pi R}\right)\left(\frac{2\mu_{\Gamma h}}{\hbar^2}\right)e^{ik_0R}, \quad (30)$$

with $k_0 = \sqrt{2\mu_{\Gamma h}(\hbar\omega - E_0)}$. Also, since $v_{Lh} \to 0$ and ${}_1F_1(0, b, z) = 1$, Eq. (20) reduces to a plane wave, $F_{\boldsymbol{kK},h}(\boldsymbol{R}) = e^{i\boldsymbol{k}\cdot\boldsymbol{R}}/\sqrt{V}$. Inserting these limit expressions into Eq. (17), we find

$$R^{\pm}_{i\to f} = \frac{2\pi}{\hbar}\frac{M_P^2 M_R^2}{V}\left(\frac{2P^2}{3}\right)D_{\Gamma L}^2\left[n_{\rm LA} + \frac{1}{2} \pm \frac{1}{2}\right]\frac{1}{V}\left(\frac{2\mu_{\Gamma h}}{4\pi\hbar^2}\right)^2 \sum_{\boldsymbol{kK}h}\left|\int_V d\boldsymbol{R} e^{-i\boldsymbol{k}\cdot\boldsymbol{R}} e^{is_{hL}(\boldsymbol{K}-\boldsymbol{k}_L)\cdot\boldsymbol{R}}\frac{e^{ik_0 R}}{R}\right|^2$$
$$\times\,\delta\left[\frac{\hbar^2 k^2}{2\mu_{Lh}} + \frac{\hbar^2(\boldsymbol{K}-\boldsymbol{k}_L)^2}{2M_{Lh}} \pm \hbar\Omega_{\rm LA} - \hbar\omega\right]. \tag{31}$$

We now change variables to

$$\boldsymbol{k}_h = s_{hL}(\boldsymbol{K}-\boldsymbol{k}_L) - \boldsymbol{k}, \quad \boldsymbol{k}_e = s_{eLh}(\boldsymbol{K}-\boldsymbol{k}_L) + \boldsymbol{k}, \tag{32}$$

so that

$$\frac{\hbar^2 k^2}{2\mu_{Lh}} + \frac{\hbar^2(\boldsymbol{K}-\boldsymbol{k}_L)^2}{2\mu_{Lh}} = \frac{\hbar^2 k_e^2}{2m_L} + \frac{\hbar^2 k_h^2}{2m_h}. \tag{33}$$

Therefore

$$R^{\pm}_{i\to f} = \frac{2\pi}{\hbar}\frac{M_P^2 M_R^2}{V}\left(\frac{2P^2}{3}\right)D_{\Gamma L}^2\left[n_{\rm LA} + \frac{1}{2} \pm \frac{1}{2}\right]\frac{1}{V}\left(\frac{2\mu_{\Gamma h}}{\hbar^2}\right)^2 \sum_{\boldsymbol{k}_e\boldsymbol{k}_h h}\left|\frac{1}{k_h^2 - k_0^2}\right|^2 \delta\left(E_{\rm ind} + \frac{\hbar^2 k_e^2}{2m_L} + \frac{\hbar^2 k_h^2}{2m_h} \pm \hbar\Omega_{\rm LA} - \hbar\omega\right), \tag{34}$$

where we have used $\int_0^\infty dR e^{ik_0 R}\sin k_h R = k_h/(k_h^2 - k_0^2)$; $\mathrm{Im}k_0 > 0$.

Converting the sums over k_e and k_h into integrals and changing variables by defining $\varepsilon = \hbar^2 k_e^2/2m_L$ and $\varepsilon' = \hbar^2 k_h^2/2m_h$, we finally obtain, after some straightforward manipulations,

$$R^{\pm}_{i\to f} = \frac{8}{3\hbar^7\pi^3} M_P^2 M_R^2 P^2 D_{\Gamma L}^2\left[n_{\rm LA} + \frac{1}{2} \pm \frac{1}{2}\right]\frac{1}{(\hbar\omega - E_0)^2}$$
$$\times \sum_h m_h^{3/2} m_L^{3/2}\int_0^{\hbar\omega - E_{\rm ind} \mp \hbar\Omega_{\rm LA}} d\varepsilon \frac{\sqrt{\varepsilon}\sqrt{\hbar\omega - E_{\rm ind} \mp \hbar\Omega_{\rm LA} - \varepsilon}}{\left[1 + \frac{\hbar\omega - E_{\rm ind} \mp \hbar\Omega_{\rm LA} - \varepsilon}{s_{e\Gamma h}(E_0 - \hbar\omega)}\right]^2}. \tag{35}$$

This expression includes an additional factor of 4 to account for valley degeneracy. The integral can be performed analytically, and we finally obtain for the absorption coefficient

$$\alpha^{\pm}_{\rm free} = \frac{4n_{op}}{3\hbar^7 c\pi^2} M_L^2 M_R^2 P^2 D_{\Gamma L}^2\left[n_{\rm LA} + \frac{1}{2} \pm \frac{1}{2}\right]\sum_h s_{e\Gamma h}^2 m_h^{3/2} m_L^{3/2}\left\{\frac{1}{\sqrt{(E_0 - \hbar\omega)}}\left[\frac{2(E_0 - \hbar\omega) + (\hbar\omega - E_{\rm ind} \mp \hbar\Omega)/s_{e\Gamma h}}{\sqrt{(E_0 - \hbar\omega) + (\hbar\omega - E_{\rm ind} \mp \hbar\Omega)/s_{e\Gamma h}}}\right] - 2\right\}. \tag{36}$$

This is exactly equivalent to Hartman's result, except that in a calculation that fully accounts for the mass anisotropy of the L valley in the conduction band, one must use $m_L^{3/2} = m_\perp m_\parallel^{1/2}$. If we now define the dimensionless variable

$$y = \frac{E_0 - \hbar\omega}{E_0 - E_{\rm ind} \mp \hbar\Omega_{\rm LA}}, \tag{37}$$

it is apparent that the nonresonant limit obtains for $y \to 1$. Expanding Eq. (36) to second order in $\eta = (1-y)/y$, one obtains the textbook result [24]:

$$\alpha^{\pm}_{\rm free} = \frac{n_{op}}{3\hbar^7 c\pi^2} M_P^2 M_R^2 P^2 D_{\Gamma L}^2\left[n_{\rm LA} + \frac{1}{2} \pm \frac{1}{2}\right]\sum_h m_h^{3/2} m_L^{3/2}\eta^2$$
$$= \frac{4n_{op}}{3\hbar^7 c\pi^2} M_P^2 M_R^2 P^2 D_{\Gamma L}^2\left[n_{\rm LA} + \frac{1}{2} \pm \frac{1}{2}\right]\sum_h m_h^{3/2} m_L^{3/2}\frac{(\hbar\omega - E_{\rm ind} \mp \hbar\Omega_{\rm LA})^2}{(E_0 - \hbar\omega)^2}. \tag{38}$$

4. Elliott limit

The indirect excitonic absorption proposed by Elliott is obtained, as indicated above, in the limit of constant denominators in Eq. (13). In this limit we have

$$\lim_{E_0/\hbar\omega\to\infty} G^h_{\hbar\omega}(\boldsymbol{R}, 0) = \frac{\delta(\boldsymbol{R})}{E_0 - \hbar\omega}, \tag{39}$$

and inserting this back into Eq. (17) we obtain

$$R^{\pm}_{i\to f} = \frac{2\pi}{\hbar}\frac{M_P^2 M_R^2}{V}\left(\frac{2P^2}{3}\right)D^2_{\Gamma L}\left[n_{\rm LA}+\frac{1}{2}\pm\frac{1}{2}\right]\frac{1}{(E_0-\hbar\omega)^2}\sum_{\lambda \boldsymbol{K} h}|F^*_{\lambda \boldsymbol{K},h}(\boldsymbol{0})|^2\delta(E_{\lambda \boldsymbol{K},h}\pm\hbar\Omega_{\rm LA}-\hbar\omega). \tag{40}$$

For the case of bound excitons, using $L^1_{n-1}(0)=n$ in Eq. (18),

$$F_{\lambda \boldsymbol{K},h}(\boldsymbol{0}) \equiv F_{n\boldsymbol{K},h}(\boldsymbol{0}) = \frac{1}{\sqrt{\pi}(n a_{BLh})^{3/2}}, \tag{41}$$

whereas for the continuum excitons we have from Eq. (20)

$$F_{\lambda \boldsymbol{K},h}(\boldsymbol{0}) \equiv F_{\boldsymbol{k}\boldsymbol{K},h}(\boldsymbol{0}) = \frac{1}{\sqrt{V}}\Gamma(1+i\nu_{Lh})e^{\pi\nu_{Lh}/2}, \tag{42}$$

where we have used ${}_1F_1(a,b,0)=1$. Inserting Eq. (41) or (42) into (40) and performing the changes of variables $\boldsymbol{k}'=\boldsymbol{K}-\boldsymbol{k}_L$, we obtain, after several straightforward steps that mimic our derivation of the resonant case,

$$\alpha^{\pm}_{\rm bound} = \frac{8\sqrt{2}n_{op}}{3\pi c\hbar^4}M_P^2M_R^2P^2D^2_{\Gamma L}\left[n_{\rm LA}+\frac{1}{2}\pm\frac{1}{2}\right]\frac{1}{(E_0-\hbar\omega)^2}\sum_{nh}\frac{M_{Lh}^{3/2}}{(n a_{BLh})^3}\sqrt{\hbar\omega-E_{\rm ind}\mp\hbar\Omega_{\rm LA}+\frac{R_{yLh}}{n^2}}. \tag{43}$$

For the case of the continuum solution, we find

$$\begin{aligned}R^{\pm}_{i\to f} = {}& \frac{2\pi}{\hbar}\frac{M_P^2M_R^2}{V}\left(\frac{2P^2}{3}\right)D^2_{\Gamma L}\left[n_{\rm LA}+\frac{1}{2}\pm\frac{1}{2}\right]\frac{1}{(E_0-\hbar\omega)^2}\\ &\times\sum_{\boldsymbol{k}\boldsymbol{k}'h}\frac{1}{\sqrt{V}}|\Gamma(1+i\nu_{Lh})|^2e^{\pi\nu_{Lh}}\delta\left(E_{\rm ind}+\frac{\hbar^2k'^2}{2M_{Lh}}+\frac{\hbar^2k^2}{2\mu_{Lh}}\pm\hbar\Omega_{\rm LA}-\hbar\omega\right),\end{aligned} \tag{44}$$

from which we obtain, using the properties of the Gamma function and converting the sums over wave vector to integrations over energy,

$$\begin{aligned}\alpha^{\pm}_{\rm continuum} = {}& \frac{8n_{op}}{3\hbar^7c\pi^3}M_P^2M_R^2P^2D^2_{\Gamma L}\left[n_{\rm LA}+\frac{1}{2}\pm\frac{1}{2}\right]\frac{1}{(E_0-\hbar\omega)^2}\\ &\times\sum_h m_h^{3/2}m_L^{3/2}\int_0^{\hbar\omega-E_{\rm ind}\mp\hbar\Omega_{\rm LA}}d\varepsilon S(\varepsilon)\sqrt{\varepsilon}\sqrt{\hbar\omega-E_{\rm ind}-\varepsilon\mp\hbar\Omega_{\rm LA}}.\end{aligned} \tag{45}$$

Here

$$S(\varepsilon) = \frac{\pi\nu_{Lh}e^{\pi\nu_{Lh}}}{\sinh(\pi\nu_{Lh})} = \frac{\pi\sqrt{R_{yLh}/\varepsilon}e^{\pi\sqrt{R_{yLh}/\varepsilon}}}{\sinh(\pi\sqrt{R_{yLh}/\varepsilon})} \tag{46}$$

is the Sommerfeld enhancement factor. In the limit of vanishing electron-hole interaction, $R_{yLh}\to 0$ and $S(\varepsilon)\to 1$, and Eq. (45) becomes Eq. (38).

C. Sphericalization approximation

1. Effective masses

Our model of indirect excitons in Ge is based on assuming that the conduction band around the L point of the BZ has an isotropic parabolic dispersion with effective mass m_L. This is a very poor approximation, since the L valley is characterized by a longitudinal mass $m_\parallel = 1.58m$ and a transverse mass $m_\perp = 0.078m$, as shown in Table I. However, as indicated above, in the noninteracting limit we recover the same absorption expression as in the anisotropic case if we use $m_L^{3/2} = m_\perp m_\parallel^{1/2}$. This suggests that we use this expression as our value of m_L in all calculations. Unfortunately, this simple approach is questionable because the indirect exciton Rydberg energies calculated with this mass are ∼7 meV for heavy holes and ∼2 meV for light holes. Experimentally, one sees a single $1s$ exciton level split into upper and lower components with binding energies of 3 and 4 meV, respectively [16]. Given our choice of an isotropic mass for the L valley, we do not expect to capture the fine structure of the excitons, but the significant differences in binding energies suggest that we may be introducing large errors in our calculation of excitonic enhancements. Thus a more systematic derivation of our spherical excitonic Hamiltonian is needed. This derivation has been provided by Altarelli and Lipari [17,18], who expanded the full anisotropic excitonic Hamiltonian as a series in which the first term is spherically symmetric. The effective masses corresponding to this spherically symmetric term are, using our notation,

$$m_L = \frac{3m_\perp m_\parallel}{2m_\parallel+m_\perp};\quad m_h = \frac{2m_{hh}m_{lh}}{m_{hh}+m_{lh}}, \tag{47}$$

and therefore these are the most appropriate masses to treat excitons in Ge using a spherical dispersion model. The corresponding binding energy is $R_{yLh}=2.3$ meV. Since there are two "sphericalized" hole bands, the sums over heavy and light holes are taken into account by simply multiplying times 2 the result obtained with Eq. (47). On the other hand, using the

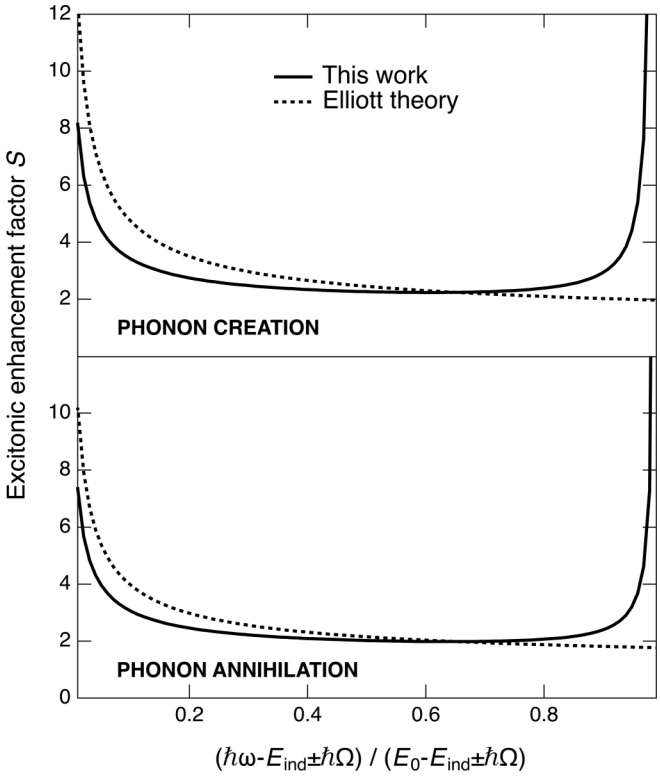

FIG. 3. Excitonic enhancement S computed as a ratio of the continuum contribution to the absorption and the absorption calculated for free electron-hole pairs. The "+" sign in the horizontal axis label applies to the case of phonon annihilation; the "–" sign to phonon creation. The solid line corresponds to the resonant excitonic model introduced here, the dotted line to Elliott's model. Note the difference of the two models as the direct gap is approached. This is because the resonant model is affected by the excitonic character of the intermediate states, whereas Elliott's model is independent of the character of these states.

definitions in Eq. (47) we find that

$$R_F \equiv \frac{m_\perp m_\parallel^{1/2} m_{hh}^{3/2} + m_\perp m_\parallel^{1/2} m_{lh}^{3/2}}{2(m_L m_h)^{3/2}} = 15.0, \qquad (48)$$

which means that in the noninteracting limit of Eq. (29), the choice of effective masses from Eq. (47) leads to an absorption coefficient that is more than one order of magnitude weaker than expected from a free electron calculation. It is then apparent that a rigorously derived spherical exciton model is inconsistent with the noninteracting limit in Ge. We must then resort to an *ad hoc* correction inspired by the continuum excitonic expression in the Elliott limit, in which the excitonic effects appear as an enhancement factor $S(\varepsilon)$. The idea is to write the absorption coefficient as

$$\alpha(\hbar\omega) = \alpha_{\text{bound}}(\hbar\omega) + S(\hbar\omega)\alpha_{\text{free}}(\hbar\omega), \qquad (49)$$

where α_{free} is given by Eq. (36) with $m_L^{3/2} = m_\perp m_\parallel^{1/2}$, and $S(\hbar\omega)$ is the ratio of Eqs. (29) and (36) using in both cases the masses in Eq. (47). These enhancement factors are shown in Fig. 3, where we also show for comparison the same enhancement factors calculated for the Elliott model. As expected, the two theories make drastically different predictions as the resonant direct gap is approached. In the resonant excitonic theory presented here, the excitonic nature of the intermediate states leads to a dramatic enhancement as E_0 is approached. In the Elliott model, as indicated above, the excitonic nature of the intermediate states is irrelevant. For α_{bound}, since Eq. (24) is proportional to $\sum_h m_L^{3/2} m_h^{3/2}$ and we want consistency between bound and continuum expressions, we compute Eq. (24) with the masses in (47) and then multiply times R_F given by Eq. (48). This approach, which by design gives the correct noninteracting limit, is used below for all comparisons with experiment.

It is interesting to discuss here why a comparable correction is far less important when computing the excitonic enhancement of direct transitions in Ge [43]. If we define a sphericalized reduced mass $\mu^{-1} = m_{e\Gamma}^{-1} + m_h^{-1}$, with m_h given by Eq. (47), we find that

$$\left(\mu_{lh}^{3/2} + \mu_{hh}^{3/2}\right)/(2\mu^{3/2}) = 1.14. \qquad (50)$$

If instead we set the above equation equal to unity, and use it to compute μ, we obtain the exact noninteracting limit while paying the price of a small 14% error in the excitonic binding energy.

2. *Final state wave functions*

In the calculation of the continuum contribution to indirect exciton absorption, we reduced the number of numerical integrations by approximating the confluent hypergeometric function of the first kind as in Eq. (25). To examine the validity of this approximation, we choose the z axis along the $\boldsymbol{k}$ vector and define the angular average:

$$\begin{aligned} {}_1\overline{F}_1(-i\nu, 1, -ikR - i\boldsymbol{k}\cdot\boldsymbol{R}) &= \frac{1}{2}\int_0^\pi d\theta \sin\theta\, {}_1F_1[-i\nu, 1, -ikR(1+\cos\theta)] \\ &= \frac{1}{2}\int_{-1}^1 du\, {}_1F_1[-i\nu, 1, -ikR(1+u)]. \end{aligned} \qquad (51)$$

Figure 4 compares the average function defined in (51) with the approximated expression in Eq. (25). We see that the agreement is very good. This means that our approximation is consistent with the use of an angular average of the exact excitonic wave function, and since the wave function is integrated over the angles in Eq. (17), the error incurred must be small when using an angular average of the wave function rather than the wave function itself. Furthermore, since the wave function in Eq. (20) is the solution of the Schrödinger equation with sphericalized effective masses, any small differences observed in calculations using the "exact" wave function on the left side of Eq. (25) or the approximation on the right-hand side may be physically meaningless.

We have also verified that the use of the Eq. (25) approximation has a negligible effect on the wave function normalization.

III. EXPERIMENT

Optical transmittance and reflectance measurements were carried out on six Ge specimens. Three of these samples were commercial optical windows from ISP Optics [44] with

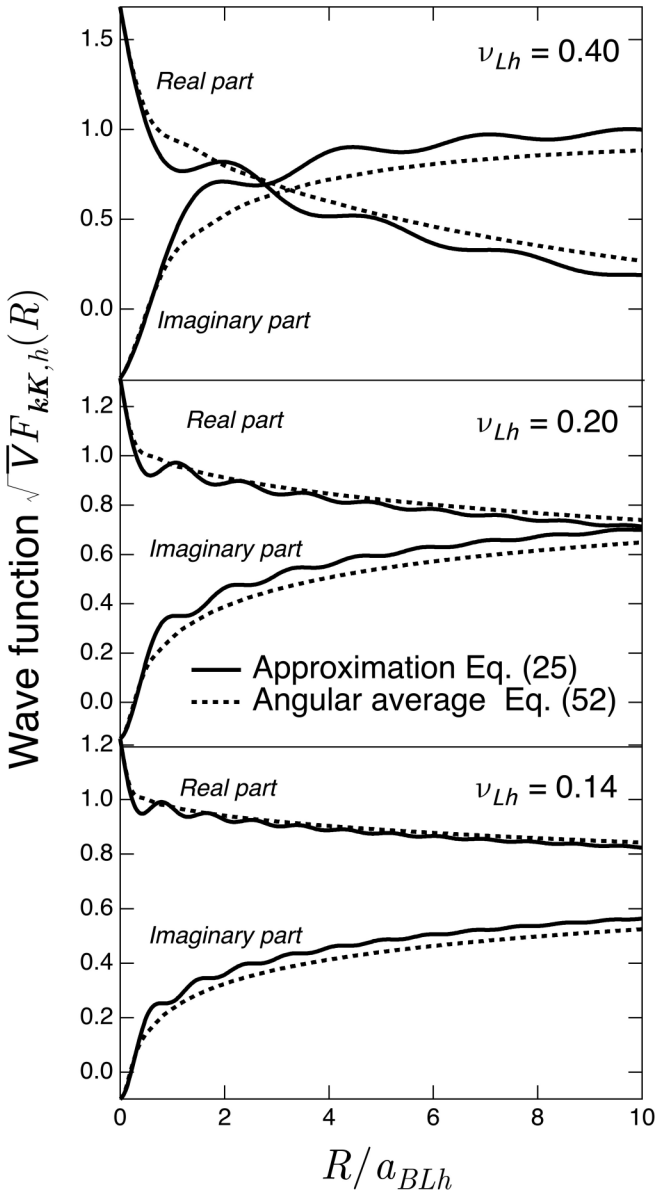

FIG. 4. Comparison of the approximate continuum exciton wave function proposed in Eq. (25) (solid line) with the angular average of the exact wave function, as in Eq. (51) (dashed line). The comparison is made for three values of the parameter ν_{Lh} covering the full range of excitonic energies.

thicknesses $d = 1.04$, 2.13, and 3.04 mm, respectively. The three remaining samples were double-sided, polished (roughness <1 nm RMS), commercial epiready Ge substrates from Umicore [45], with $d = 0.175$ mm. The Umicore substrates have an extremely low impurity concentration below $2 \times 10^{10}\text{cm}^{-3}$, corresponding to a resistivity higher than 57 Ω cm. We used a PerkinElmer Lambda 1050 spectrophotometer equipped with an InGaAs sphere detector to measure the regular transmittance $\mathcal{T}$ under normal incidence. The specular reflectance $\mathcal{R}$ was measured at near-normal incidence ($8.0^\circ \pm 0.25^\circ$ incidence) using a PerkinElmer Lambda 900 spectrophotometer equipped with a VW directional reflectance accessory (PE L6310200) and a PbS sphere detector. The use of sphere-based detectors for these optical measurements reduces uncertainties due to detector nonlinearity, nonuniformity, and inter-reflection effects. The measurements were performed at an average temperature $T = 301$ K, as recorded using a calibrated digital thermometer (Fluke Model 1529-R) with an uncertainty of $\pm 0.0025\,^\circ$C at 25 °C. The thermometer was mounted inside the sample compartment. The temperature drift during any individual measurement was 3 K or less. The regular transmittance measurements are traceable to the well-characterized NRC Reference Spectrophotometer [46]. The absolute VW (Strong method) specular reflectance measurements were confirmed by comparison with a high reflectance dielectric laser mirror optimized for 2037 nm [47].

For all wavelengths probed, $d \gg \lambda$, so that $\mathcal{R}$ and $\mathcal{T}$ can be obtained by adding incoherently the contributions from the two air-sample interfaces. We then obtain

$$\begin{aligned}\mathcal{R} &= R + T\exp(-\alpha d)R\exp(-\alpha d)T \\ &\quad + T^2R^3\exp(-4\alpha d) + \cdots \\ &= \frac{R[1+(1-2R)\exp(-2\alpha d)]}{1-R^2\exp(-2\alpha d)},\end{aligned} \tag{52}$$

where R and T are the reflectance and transmittance at a single air-sample interface and α is the absorption coefficient. Similarly, the sample's absorptance $\mathcal{A} = 1 - R - \mathcal{T}$ is given by

$$\begin{aligned}\mathcal{A} &= T[1-\exp(-\alpha d)][1 + R\exp(-\alpha d) \\ &\quad + R^2\exp(-2\alpha d) + \cdots] \\ &= \frac{(1-R)[1-\exp(-\alpha d)]}{1-R\exp(-\alpha d)}.\end{aligned} \tag{53}$$

The desired absorption coefficient can be obtained from the experimental $\mathcal{R}$ and $\mathcal{A}$. We define

$$z \equiv \exp(-\alpha d), \tag{54}$$

so that Eqs. (53) and (52) can be rewritten as

$$z = \frac{\mathcal{A} - 1 + R}{\mathcal{A}R - 1 + R}, \tag{55}$$

$$(2-\mathcal{R})z^2R^2 - (1+z^2)R + \mathcal{R} = 0. \tag{56}$$

This system can be easily solved by iteration. We can first assume $R = \mathcal{R}$—which corresponds to the high-absorption limit of Eq. (52)—and calculate z from Eq. (55). Next we insert this z into Eq. (56) and solve for R, which is then inserted back into Eq. (55) to continue the iterative process. Alternatively, we can start the iteration process by taking the low-absorption limit of Eq. (52), $R = \mathcal{R}/(2-\mathcal{R})$. For typical values of the experimental quantities, virtually perfect convergence is reached in as few as three iterations starting from either limit. Results are shown in Fig. 5, where we include only one of the $d = 0.175$ mm samples, as the others give a virtually identical absorption coefficient. As expected, we see from Fig. 5(a) that the $d = 0.175$ mm sample and even the $d = 1.04$ mm sample are too thin for accurate measurements near the absorption edge, where the results converge for $d > 2$ mm. At the other end of the spectrum, we observe that only the $d = 0.175$ mm samples can be used to reach the direct gap, so that the samples with this thickness are crucial

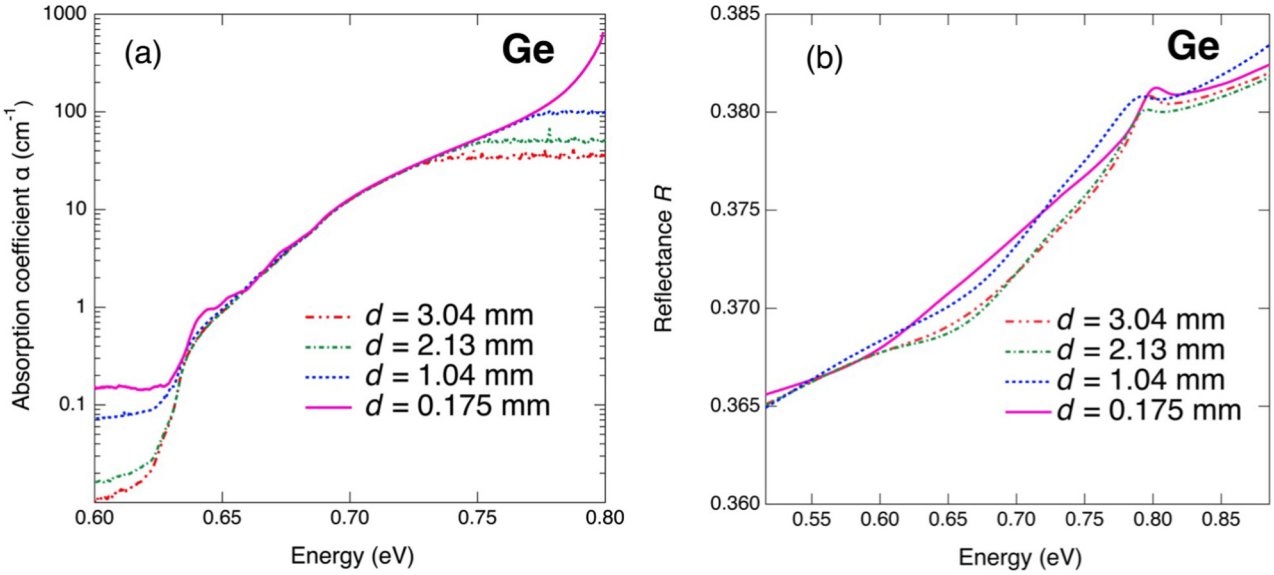

FIG. 5. (a) Absorption coefficient α extracted from the experimental data by solving Eqs. (55) and (56) iteratively. (a) Corresponding air-germanium interface reflectance obtained by the same procedure, after smoothing as described in the text.

to study the resonant indirect absorption. At intermediate energies, the absorption coefficients from all samples are in excellent agreement, indicating that errors are very small and that the method used to extract the absorption is robust. The corresponding reflectances are shown in Fig. 5(b). Smoothing has been applied to the reflectance curves to eliminate instrumentally induced noise that appears between 0.65 and 0.70 eV. The observed noise in R can be traced back not only to noise in the raw $\mathcal{R}$ data but also to residual fluctuations in the transmittance, which has the steepest slope in this spectral range. The reflectance curves are also in excellent agreement with each other, with the largest discrepancies not exceeding 0.5%. The local maxima near 0.80 eV are associated with the direct gap E_0. Fluctuations in the position of these local maxima, within a range of about 10 meV, are apparent in the data. Energy shifts of this magnitude are too large to be due to thermal drift, since a temperature change $\Delta T = 3\,\mathrm{K}$ corresponds to $\Delta E_0 = -1.3\,\mathrm{meV}$ [48]. More likely, the shifts are due to residual doping levels. For example, a doping level of $10^{16}\mathrm{cm}^{-3}$ corresponds to a band gap renormalization of -5 meV [49]. This interpretation is consistent with the fact that in the high-resistivity $d = 0.175\,\mathrm{mm}$ samples the E_0 peak is sharper and appears at the highest energy.

Figure 6 compares our measured absorption with data in the literature. Macfarlane *et al.* [7] computed the absorption coefficient from transmission measurements on three Ge specimens. The reflectance was not measured independently. Instead, its value below the absorption edge was deduced from transmission measurements assuming no residual absorption, and taken as independent of energy. Pankove and Aigrain [8] used a similar approach, setting $R = 0.36$. We see that the Macfarlane curve agrees very well with our data except for a shift to higher energy by about 5 meV. This corresponds to a temperature difference $\Delta T = -11\,\mathrm{K}$, in very good agreement with the actual difference $\Delta T = -10\,\mathrm{K}$ between the two data sets. The dispersion of the indirect absorption as the direct gap is approached is slightly different in the Pankove-Aigrain data. This is not due to their assumption of constant reflectivity, but rather to differences in the experimental transmittances. We note, however, that the assumption of constant reflectance must be dropped if the absorption coefficient is to be determined with a small fractional error over the entire spectral range between the indirect and direct gaps—as done here. For example, if we were to process our data using the Pankove-Aigrain

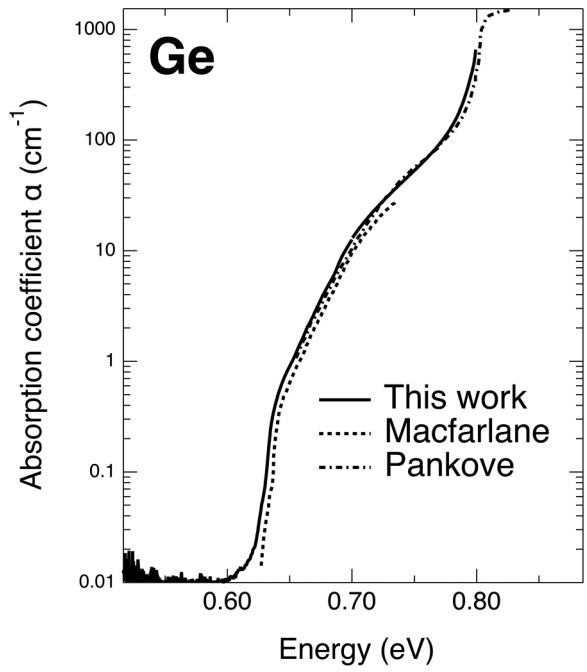

FIG. 6. The solid line shows the measured absorption in pure Ge at 301 K. For $E < 0.7$ eV we use data from the $d = 3.04\,\mathrm{mm}$ sample, and for $E \geqslant 0.7$ we use data from a $d = 0.175\,\mathrm{mm}$ sample. The dotted line corresponds to measurements by Macfarlane *et al.* (Ref. [7]) at 291 K, and the dash-dotted line is from Pankove and Aigrain (Ref. [8]).

assumption $R = 0.36$, the difference would be negligible near the direct gap, but more than a factor of 2 near the onset of absorption at the indirect gap. In other words, simultaneous measurements of transmittance and reflectance, as presented here, are critical to obtain reliable values of the absorption coefficient over the entire spectral range.

IV. COMPARISON OF THEORY AND EXPERIMENT

A. Issues in the extreme resonant regime

The absorption data just described can be compared with the theoretical predictions using Eq. (49). However, in the extreme resonant limit very close to E_0 the analysis is complicated by a number of effects not included in the theory developed in Sec. II. At an energy $\hbar\Omega_O \sim 36$ meV below E_0, an additional absorption channel becomes possible, namely, optical-phonon-assisted direct transitions. Attempts to observe laser-induced cooling in direct gap semiconductors are based on this mechanism [50]. Phonon-assisted direct transitions are allowed because the optical phonons couple the light- and heavy-hole bands via the electron-phonon interaction. The calculation of this process is quite similar to the indirect absorption theory described in Sec. II, and it is sketched in Appendix A. As seen in Fig. 9, the expected phonon-induced direct gap absorption is weak compared to indirect absorption, but for completeness it will be added to our theoretical model.

An additional issue in the extreme resonant limit is that the contribution from first-order direct gap absorption can only be ignored at very low temperatures, but at room temperature the direct absorption edge is broadened, and its low-energy tail will overlap with the indirect absorption. Since a tail from a first-order process might be comparable in strength with the second-order indirect absorption, care must be exercised in analyzing data in this energy range. A possible way to extract the "true" indirect absorption would be to fit the direct gap absorption with a theoretical expression and subtract the fit curve from the experimental absorption below the direct gap. The difference should correspond to the bona fide indirect absorption. However, our theoretical expressions for indirect absorption are not adequate for analyzing the resulting data because they do not include lifetime effects. Since Γ-point excitons are the final states in direct gap absorption and the intermediate states in indirect gap absorption, consistency requires that the same lifetime broadening effects be included in our theoretical account of direct and indirect absorption. Furthermore, lifetime effects in Γ-point excitons are actually more important for indirect absorption, because our expressions [see, for example, Eq. (36)] *diverge* for $\hbar\omega \to E_0$. Accordingly, broadening affects not only the line shape but also the strength of the resonant indirect absorption. Second-order perturbation theory becomes inadequate in this limit, and a rigorous theoretical approach requires a treatment beyond the scope of this paper. We then adopt a more modest approach that consists in estimating a threshold energy below E_0 at which broadening effects become small, and excluding from the analysis all photon energy above this threshold.

B. Direct absorption and lifetime effects

The threshold energy below which it is "safe" to use the theory of Sec. II, which does not incorporate lifetime effects, can be estimated from a theoretical analysis of direct gap absorption. Figure 7 shows room-temperature experimental data from Ref. [43], and a fit with a theoretical expression discussed in Refs. [43,51]. The theoretical calculation is based on the Elliott analysis for direct transitions [14,20]. The effect of broadening is accounted for by simply convoluting the calculated imaginary part of the dielectric function with a normalized Gaussian or Lorentzian. The only adjustable parameters are the temperature, which determines the exact value of E_0 [48], and the broadening. Notice that there is no *ad hoc* "amplitude" parameter, so that the strength of the absorption is predicted by theory. It is apparent from Fig. 7 that Gaussian broadening leads to remarkable agreement with experiment. The fit values in this case are 0.015 meV for the broadening [full width at half maximum (FWHM) of the Gaussian] and a temperature $T = 300$ K. Lorentzian broadening, on the other hand, fails to reproduce the experimental line shape. The deviation between theory and experiment at higher energy is due to band nonparabolicity, which is not included in the model. Note that the agreement between theory and experiment is good for absorption values as high as $\alpha = 5000\,\mathrm{cm}^{-1}$. This insures that the fit is completely dominated by the direct absorption.

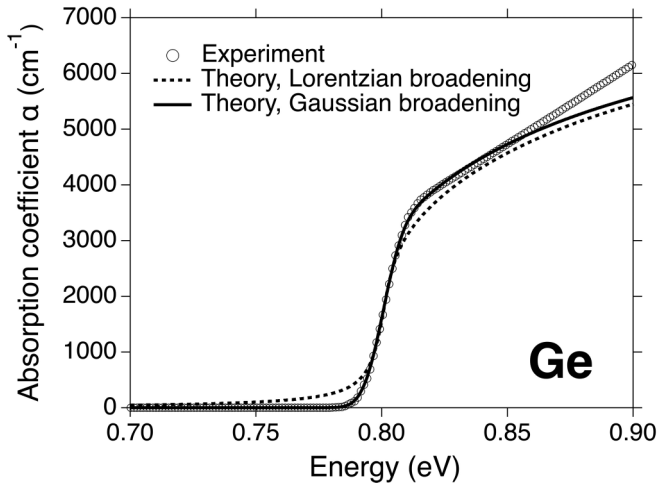

FIG. 7. Theoretical fit of the room-temperature direct gap in Ge with the theory described in Ref. [42]. The only adjustable parameters are the band gap energy and the magnitude of the broadening.

Based on the fit of the direct absorption edge in Fig. 7, we define the threshold energy for neglecting broadening effects as the energy at which the tail of the direct absorption fit accounts for less than 2% of the experimental absorption at this energy. We find that this condition is satisfied 24 meV below E_0.

C. Indirect absorption fits

The above considerations suggest that the theory developed in the previous sections should be valid at least up to an energy $\hbar\omega \sim 0.78$ eV. For actual fits, however, we need to consider the fact that the absorption near this energy is a rapidly increasing function of photon energy, so that the fit will be dominated by the highest energy values unless we introduce some data-point weight factors that depend on energy. To

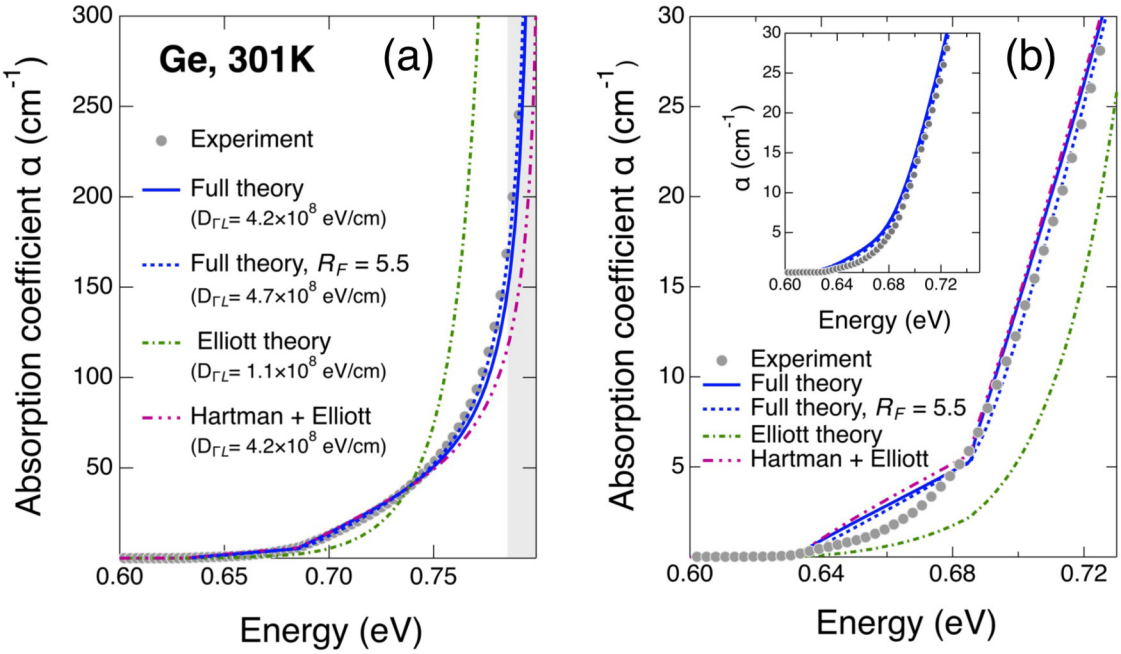

FIG. 8. (a) Circles: experimental absorption coefficient of Ge in the spectral range between the indirect and direct band gaps. Only one-fifth of the experimental points are shown to improve visualization. Solid blue line: fit with the theory described in this paper, with $D_{\Gamma L}$ as the sole adjustable parameter. Dotted blue line: same as the solid blue line but using R_F from Eq. (48) as an additional adjustable parameter. Dash-dotted green line: fit with full Elliott model that neglects the energy dependence of the intermediate states. Dash-double-dotted purple line: fit with a hybrid model that combines Hartman's theory with Elliott's excitonic enhancement model. In all cases the fit value of the deformation potential is indicated in the legend. (b) Same as (a) but showing the detail at the onset of absorption. The inset shows the calculated solid blue line of the main panel convoluted with a Gaussian with a FWHM of 0.015 eV to simulate lifetime broadening.

avoid this complication we simply fit the theoretical models to the experimental absorption data for energies $\hbar\omega < 0.75$ eV. Therefore, the agreement between theory and experiment beyond this energy will depend on the quality of the predicted line shapes. In particular, this approach will allow us to verify if the resonant excitonic enhancement predicted by our model (Fig. 3) can be observed experimentally. Furthermore, since the absorption is very small as the low-energy end of the spectral range is approached, its values near this limit do not affect the fit in any substantial way, so that the agreement between the fit and the experimental curve near the onset of absorption is also a test of the quality of the predicted photon-energy dependence of the absorption coefficient.

The fit with our full model is shown as a solid blue line in Fig. 8(a). The curve is computed using Eq. (49) and we obtain a fit value $D_{\Gamma L} = (4.2 \pm 0.1) \times 10^8$ eV/cm. This is, within error, the same as the value $D_{\Gamma L} = (4.3 \pm 0.1) \times 10^8$ eV/cm obtained in I using a slightly different energy range for the fit. The onset of absorption at the lowest energies is shown on a different scale in Fig. 8(b). The lowest-energy threshold corresponds to phonon-annihilation processes, and the kink at 0.685 eV marks the onset of phonon-creation absorption. The kink is not obvious in the experimental data, most likely as a result of lifetime broadening. To confirm this explanation we show in the inset the calculated absorption after convolution with a Gaussian with a FWHM = 0.015 eV, the broadening used above for direct gap absorption. We see that the resulting curve shows a line shape very similar to the experimental data. A second fit with our theoretical model was performed using the factor R_F in Eq. (48) as an additional adjustable parameter. This is motivated by the fact that the correction of the bound exciton contribution by this factor is arguably the least justified assumption in our model.

We show two additional theoretical fits in Fig. 8 to help understand the physics involved. In all cases, the fit parameter value is shown in the legend. The dash-dotted green line was computed using the Elliott model following Eq. (49), i.e., taking α_{free} as the textbook expression in Eq. (38); computing the excitonic enhancement $S(\hbar\omega)$ using the Elliott exciton model, Eq. (45); and adding the bound exciton contribution from Eq. (43). The dash-double-dotted purple line corresponds to a hybrid approach in which α_{free} is taken from the Hartman model in Eq. (36), but using the excitonic enhancement $S(\hbar\omega)$ from Elliott's model (dashed lines in Fig. 3). This is logically inconsistent, as stressed above, but useful for understanding the different contributions to the absorption.

V. DISCUSSION

The solid blue line in Figs. 8(a) and 8(b) is in very good agreement with the experimental data over the entire spectral range of the measurement, with a fit $D_{\Gamma L}$ that is equal to the independently determined value of this parameter. In other words, our theory makes it possible to predict indirect absorption quantitatively without using *any* adjustable parameter. It is quite remarkable that the relative error of the theoretical prediction is small over two orders of magnitude in the value of the absorption. The largest discrepancy occurs near the energy of the indirect band gap, close to the spectral region where the excitonic effects at low temperature cannot be

explained with the sphericalization approach used here [15,16]. The small remaining discrepancy at higher energies can be further reduced by considering the mass ratio R_F in Eq. (48) as an adjustable parameter. This factor is used to correct the bound exciton absorption, and it is more difficult to justify than the approximations used to deal with the continuum contribution. This is because the latter must give α_{free} in the limit of vanishing excitonic Coulomb interaction, but the former simply approaches zero. The result of this exercise is shown as a blue dotted line in Fig. 8. The fit deformation potential $D_{\Gamma L} = 4.7\,\text{eV}$ is still reasonable, but the mass ratio $R_F = 5.5$ has decreased by almost a factor of 3 relative to the ansatz in Eq. (48). It is unclear if one can assign a definite physical meaning to this reduced value of R_F. It could be simply due to the fact that our theory neglects band nonparabolicity, which would then by accommodated in an effective way by adjusting R_F. However, caution is needed in embracing this or any other interpretation because the bound exciton contribution is small, and a very large change in R_F only induces modest changes in the predicted absorption, as seen in Fig. 8.

The green dash-dotted line corresponding to Elliott's model, the "standard" approach prior to our work, is clearly in very poor agreement with experiment. The fit $D_{\Gamma L} = 1.1\,\text{eV}$ is too small but probably meaningless in view of the dramatic difference in line shape between theory and experiment. Since the absorption is dominated by the continuum contribution, which is written in Eq. (49) as $S(\hbar\omega)\alpha_{\text{free}}(\hbar\omega)$, it is instructive to investigate how these two factors combine to improve the agreement with theory as we move from the Elliott model to the resonant theory developed here. For this purpose, we show as a dash-double-dotted purple line a hybrid fit consisting of using the Hartman model in Eq. (36) for $\alpha_{\text{free}}(\hbar\omega)$ together with the excitonic enhancement $S(\hbar\omega)$ calculated within Elliott's model. We see that the fit is vastly improved relative to the dash-dotted green line, indicating that a correct resonant theory for $\alpha_{\text{free}}(\hbar\omega)$ is the main factor contributing to the agreement between theory and experiment. The Hartman theory in Eq. (36), with its $1/\sqrt{E_0 - \hbar\omega}$ resonant prefactor for $\alpha_{\text{free}}(\hbar\omega)$, is far superior to the textbook expression in Eq. (38), which features a $1/(E_0 - \hbar\omega)$ resonant prefactor. On the other hand, we notice that the dash-dotted green line deviates from the experimental absorption at high energies. This is precisely the energy range where the excitonic enhancement $S(\hbar\omega)$ calculated with a resonant excitonic theory departs from Elliott's model the most, as seen in Fig. 3. The latter is not affected by the excitonic character of the intermediate states, whereas the former shows a pronounced resonance as a result of this character. Therefore, our data confirm that a consistent model of indirect absorption in Ge, which considers the energy dependence of the intermediate states both in the calculation of $\alpha_{\text{free}}(\hbar\omega)$ and $S(\hbar\omega)$, is needed for an accurate account of the experimental results.

VI. CONCLUSION

In summary, we have presented experimental results for the optical absorption in Ge covering the entire spectral range between the indirect and direct gap and we have introduced a theory of resonant indirect optical absorption to explain the result. The main ingredient of the theoretical approach is a realistic account of the energy dependence of the intermediate states, which in Ge, unlike the case of Si, cannot be neglected. The resulting theory is in excellent agreement with experiment using independently determined parameters.

The theory presented here does not include lifetime broadening. Near the onset of absorption this broadening can be incorporated in a phenomenological way by convoluting the calculated absorption with a suitable broadening function, as done in the inset in Fig. 8(a). Near the resonant direct gap E_0, however, the lifetime broadening of E_0 plays a more critical role because the predicted absorption diverges at E_0, so that lifetime effects control not only the precise line shape but also the absorption strength. The validity of second-order perturbation theory is questionable in this limit, while a more rigorous theory may be substantially more complicated. In this context, we note that the lifetime broadening of E_0 cannot be accounted for by adding a small imaginary part to the energy. This is equivalent to Lorentzian broadening, which, as shown in our analysis of direct gap transitions, fails to account for the experimental data. Even at a phenomenological level, a more sophisticated theory of broadening increases the mathematical complexity considerably, even for direct transitions [52]. We have circumvented this problem by avoiding the spectral region where broadening effects are likely to be significant. However, this approach will break down in the case of $Ge_{1-y}Sn_y$ alloys, for which the separation between the direct and indirect gaps can be reduced and reversed [53]. In these alloys, resonant indirect transitions may affect the optical gain in laser structures and require further experimental and theoretical work.

The absorption model presented here should be extensible to indirect gap III-V semiconductors such as AlAs, GaP, and related alloys [54]. While the Ge case is simpler, since a single resonant channel can be isolated, III-Vs should display stronger excitonic effects that may amplify the differences between the conventional Elliott treatment and the more rigorous resonant exciton model. Finally, our absorption model also provides the tools to calculate indirect gap emission in all of these materials using van Roosbroeck-Schockley-type expressions [55]. This is of particular interest in Ge and $Ge_{1-y}Sn_y$ alloys in which the relative strengths of direct and indirect gap emission can be used to monitor the transition from indirect to direct gap semiconductor [56].

ACKNOWLEDGMENT

This work was supported by the AFOSR under Grant No. FA9550-17-1-0314.

APPENDIX A: PHONON-ASSISTED DIRECT GAP TRANSITION

The indirect absorption calculated in Sec. II is mediated by LA phonons that couple conduction band states at Γ and L. Optical phonons, on the other hand, couple the valence band states, and therefore optical-phonon-assisted absorption becomes possible just below the direct gap E_0. This absorption is usually neglected because it is expected to be much

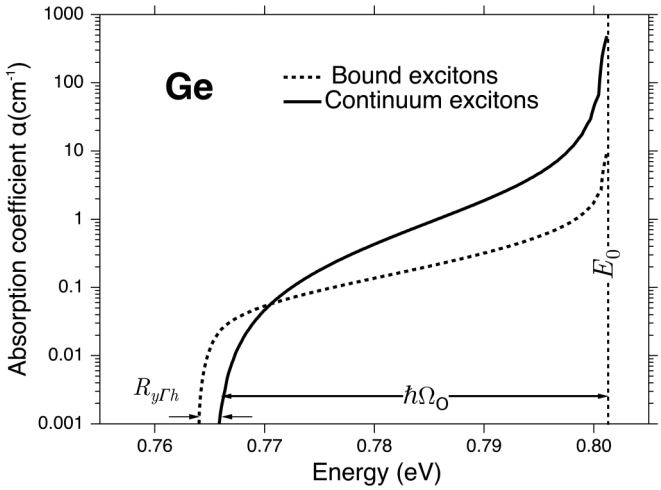

FIG. 9. Calculated phonon-assisted direct absorption coefficient of Ge using parameters from Table I. The dotted line shows the bound exciton contribution, from Eq. (A10), and the solid line corresponds to the continuum exciton contribution, Eq. (A15). In both cases we use effective masses from Eq. (47).

weaker than the allowed direct gap absorption, although it has played a role in laser cooling proposals [50]. The purpose of this work, however, is to model indirect gap absorption with emphasis on the resonant enhancement that occurs as the incident photon energy approaches the direct gap, and therefore it is important to compare the relative strength of the LA-phonon-assisted indirect absorption with optical-phonon-assisted direct absorption. The coupling of optical phonons with the valence band can be described by the Hamiltonian

$$H_{eP} = \frac{M_O}{\sqrt{V}}\left(\frac{d_0}{a_0}\right)\sum_{\boldsymbol{q}s}\sum_{v'v\boldsymbol{k}} v^\dagger_{\boldsymbol{k}+\boldsymbol{q},v'} v_{\boldsymbol{k},v}\{b(\boldsymbol{q}s) - b^\dagger(-\boldsymbol{q}s)\} \times \sum_\alpha M_{v'v}(\alpha)\hat{e}_s(\alpha); \quad M_O = \sqrt{\frac{\hbar}{2\rho\Omega_O}}, \tag{A1}$$

where Ω_O is the frequency of the optical phonons, d_0 the optical phonon deformation potential, and a_0 the cubic lattice parameter. Note that for historical reasons the deformation "potential" in Eq. (7) is defined with units of eV/cm, but the deformation "potential" in Eq. (A1) has units of eV. As in the case of Eq. (7), we neglect the wave-vector dependence of Ω_O and d_0. The index s represents the three optical phonon branches degenerate at Γ, and $\hat{e}_s(\alpha)$ is the α-Cartesian component of the unit phonon polarization vector. The sum over α runs over the Cartesian coordinates, with the matrices M given by

$$M_{v'v}(x) = \begin{pmatrix} 0 & -i & 0 & 0 \\ i & 0 & 0 & 0 \\ 0 & 0 & 0 & i \\ 0 & 0 & -i & 0 \end{pmatrix};$$
$$M_{v'v}(z) = \begin{pmatrix} 0 & 0 & 0 & -i \\ 0 & 0 & -i & 0 \\ 0 & i & 0 & 0 \\ i & 0 & 0 & 0 \end{pmatrix};$$
$$M_{v'v}(y) = \begin{pmatrix} 0 & 1 & 0 & 0 \\ 1 & 0 & 0 & 0 \\ 0 & 0 & 0 & -1 \\ 0 & 0 & -1 & 0 \end{pmatrix}, \tag{A2}$$

where $v = 1, 2, 3, 4$ as in Eq. (2). It is easy to see by inspection of these matrices that the interaction only couples light-hole with heavy-hole states, so that in a phonon-assisted absorption process mediated by this interaction, a final state with a hole in a heavy-hole state requires an optical transition from a light-hole state to the conduction band, and vice versa. We are interested mainly in phonon-annihilation processes that enable optical absorption below the direct gap E_0. For this, the relevant electron-phonon matrix element becomes, using Eq. (A1),

$$\langle G|b^\dagger_{\boldsymbol{q}L0} d_{\lambda\boldsymbol{K},\sigma v} H_{eL} d^\dagger_{\lambda'\boldsymbol{0},\sigma'v'}|G\rangle = -M_O\left(\frac{d_0}{a_0}\right)[n_O] v_c \delta_{\sigma\sigma'}\delta_{-\boldsymbol{q},\boldsymbol{K}} \sum_{\boldsymbol{R}} F^*_{\lambda\boldsymbol{K},\sigma v}(\boldsymbol{R}) F_{\lambda'\boldsymbol{0},\sigma v'}(\boldsymbol{R}) e^{-is_{e\Gamma v}\boldsymbol{K}\cdot\boldsymbol{R}} \sum_\alpha M_{v'v}(\alpha)\hat{e}_O(\alpha). \tag{A3}$$

From Fermi's golden rule we then obtain

$$R^-_{i\to f} = \frac{2\pi}{\hbar}\frac{M_O^2 M_R^2}{V}\left(\frac{d_0}{a_0}\right)^2[n_O] \times \sum_{s\boldsymbol{q},\lambda\boldsymbol{K},\sigma v}\left|\sum_{\lambda',v'}\frac{\delta_{-\boldsymbol{q},\boldsymbol{K}} v_c \sum_\beta F^*_{\lambda\boldsymbol{K},\sigma v}(\boldsymbol{R}) F_{\lambda'\boldsymbol{0},\sigma v'}(\boldsymbol{R}) e^{-is_{e\Gamma v}\boldsymbol{K}\cdot\boldsymbol{R}} \sum_\alpha M_{v'v}(\alpha)\hat{e}_O(\alpha) P_{\sigma v'} F^*_{\lambda'\boldsymbol{0},\sigma v'}(\boldsymbol{0})}{\hbar\omega - E_{\lambda'\boldsymbol{0},\sigma v'}}\right|^2 \delta(E_{\boldsymbol{q}s,\lambda\boldsymbol{K},\sigma v} - \hbar\omega). \tag{A4}$$

We now observe that for the sum over s we can take $\hat{e}_O = (1,0,0)$, $\hat{e}_O = (0,1,0)$, and $\hat{e}_O = (0,0,1)$. For either of these three cases we find that for a given state v corresponding to light or heavy holes, Eq. (A2) implies that the only nonzero matrix elements occur when v' corresponds to the opposite type of hole, and in that case $|\sum_\alpha M_{v'v}(\alpha)\hat{e}_O(\alpha)| = 1$. Furthermore, when we perform the sum over σ we find from Eq. (6) that each $v\uparrow / v\downarrow$ pair contributes $P^2/3$, and since there are two heavy-hole and two light-hole states giving exactly the same expression we can simply write (A4) as

$$R^-_{i\to f} = \frac{6\pi}{\hbar}\frac{M_O^2 M_R^2}{V}\left(\frac{d_0}{a_0}\right)^2\left(\frac{2P^2}{3}\right)[n_O]\sum_{\lambda\boldsymbol{K},h}\left|\sum_{\boldsymbol{R}} F^*_{\lambda\boldsymbol{K},h}(\boldsymbol{R}) e^{-is_{e\Gamma h}\boldsymbol{K}\cdot\boldsymbol{R}}\sum_{\lambda'}\frac{F^*_{\lambda'\boldsymbol{0},h'}(\boldsymbol{0}) F_{\lambda'\boldsymbol{0},h'}(\boldsymbol{R})}{\hbar\omega - E_{\lambda'\boldsymbol{0},h'}}\right|^2 \delta(E_{\lambda\boldsymbol{K}h} + \hbar\Omega_O - \hbar\omega), \tag{A5}$$

where h now acquires only two values: either heavy or light hole, and h' is the opposite type of hole. We have also multiplied times 3 because we obtain the same result for each of the threefold degenerate phonons at the Γ point. Using the Green's function definition in Eq. (14), this becomes

$$R^{-}_{i\to f} = \frac{6\pi}{\hbar}\frac{M_O^2 M_R^2}{V}\left(\frac{d_0}{a_0}\right)^2\left(\frac{2P^2}{3}\right)[n_O]\sum_{\lambda \boldsymbol{K},h}\left|\int d\boldsymbol{R}\, F^*_{\lambda \boldsymbol{K},h}(\boldsymbol{R})e^{-is_{e\Gamma h}\boldsymbol{K}\cdot\boldsymbol{R}}G^{h'}_{\hbar\omega}(\boldsymbol{R},\boldsymbol{0})\right|^2\delta(E_{\lambda \boldsymbol{K}h}+\hbar\Omega_O-\hbar\omega). \tag{A6}$$

To compute this expression we use for bound excitonic states, in analogy with Eq. (18),

$$F_{\lambda \boldsymbol{K},h}(R)\equiv F_{n\boldsymbol{K},h}(R)=\frac{1}{\sqrt{\pi}(na_{B\Gamma h})^{3/2}}\frac{1}{n}e^{-\rho/2}L^1_{n-1}(\rho);\quad \rho=\frac{2R}{\kappa a_{B\Gamma h}};\quad a_{BLh}=\frac{\hbar}{\sqrt{2\mu_{\Gamma h}R_{y\Gamma h}}}. \tag{A7}$$

For continuum excitons we have, in analogy with Eq. (20) [42],

$$F_{\lambda \boldsymbol{K},h}(\boldsymbol{R})\equiv F_{\boldsymbol{k}\boldsymbol{K},h}(\boldsymbol{R})=\frac{1}{\sqrt{V}}\Gamma(1+i\nu_{\Gamma h})e^{\pi\nu_{\Gamma h}/2}e^{i\boldsymbol{k}\cdot\boldsymbol{R}}{}_1F_1(-i\nu_{\Gamma h},1,-ikR-i\boldsymbol{k}\cdot\boldsymbol{R}), \tag{A8}$$

with

$$\nu_{\Gamma h}=\sqrt{\frac{R_{y\Gamma h}}{\hbar^2k^2/2\mu_{\Gamma h}}}. \tag{A9}$$

The bound exciton expression then becomes, following steps very similar to the corresponding calculation for indirect gap absorption,

$$\alpha^{-}_{\text{bound}}=\frac{128n_{op}}{\hbar^7c}M_O^2M_R^2P^2\left(\frac{d_0}{a_0}\right)^2[n_O],$$
$$\times\sum_h m_e^{3/2}m_h^{3/2}\sum_n\frac{R_{y\Gamma h}^{-1/2}}{n^5}\sqrt{\hbar\omega-E_0+\frac{R_{y\Gamma h}}{n^2}+\hbar\Omega_O}\left|H_{\Gamma nh}\left[\frac{\sqrt{2M_{\Gamma h}\left(\hbar\omega-E_0+\frac{R_{y\Gamma h}}{n^2}+\hbar\Omega_O\right)}}{\hbar^3}\right]\right|^2, \tag{A10}$$

where

$$H_{\Gamma nh}(k)=\frac{R_{y\Gamma h}}{s_{e\Gamma h}K}\int dR\,R\sin(s_{e\Gamma h}KR)G^{h'}_{\hbar\omega}(R,\boldsymbol{0})e^{-\frac{R}{na_{B\Gamma h}}}L^1_{n-1}\left(\frac{2R}{na_{B\Gamma h}}\right). \tag{A11}$$

Figure 9 shows the calculated absorption, using the masses in Eq. (47). For the continuum component, we obtain

$$R^{+}_{i\to f}=\frac{6\pi}{\hbar}\frac{M_O^2M_R^2}{V}\left(\frac{d_0}{a_0}\right)^2\left(\frac{2P^2}{3}\right)[n_O]\frac{1}{V}\sum_{\boldsymbol{k}\boldsymbol{K},h}\frac{16\pi^2}{R^2_{y\Gamma h}}|J(k,K,\theta)|^2\delta\left(E_0+\frac{\hbar^2k^2}{2\mu_{\Gamma h}}+\frac{\hbar^2K^2}{2M_{\Gamma h}}+\hbar\Omega_O-\hbar\omega\right), \tag{A12}$$

where θ is the angle between the vectors $\boldsymbol{k}$ and $\boldsymbol{K}$ and we have defined the dimensionless quantity

$$J(k,K,\theta)=\frac{R_{y\Gamma h}\Gamma(1+i\nu)e^{\pi\nu/2}}{k_e}\int dR\,RG^{h'}_{\hbar\omega}(R,\boldsymbol{0}){}_1F^*_1(-i\nu,1,-ikR)\sin k_eR, \tag{A13}$$

with

$$k_e^2=k^2+s^2_{e\Gamma h}K^2+2s_{e\Gamma h}kK\cos\theta. \tag{A14}$$

Following steps very similar to the derivation of indirect gap absorption, we finally obtain

$$\alpha^{-}_{\text{continuum}}=\left(\frac{16}{\pi\hbar^7}\right)M_O^2M_R^2\left(\frac{d_0}{a_0}\right)^2P^2[n_O]\sum_h\frac{m_{e\Gamma}^{3/2}m_h^{3/2}}{R^2_{y\Gamma h}}\int_0^{\hbar\omega-E_0+\hbar\Omega_O}d\varepsilon\sqrt{\varepsilon}\sqrt{\hbar\omega-E_0+\hbar\Omega_O-\varepsilon}$$
$$\times\int_0^\pi d\theta\sin\theta|J(k(\varepsilon),K(\hbar\omega-E_0+\hbar\Omega_O-\varepsilon),\theta)|^2. \tag{A15}$$

In the limit of vanishing electron-hole interaction this expression becomes

$$\alpha^{-}_{\text{free}}=\frac{n_{op}}{\hbar^7c\pi^2}M_R^2M_O^2P^2\left(\frac{d_0}{a_0}\right)^2[n_O]\frac{1}{\sqrt{(E_0-\hbar\omega)}}\sum_h s^2_{e\Gamma h'}(m_hm_{e\Gamma})^{3/2}\left\{\frac{2(E_0-\hbar\omega)+(\hbar\omega-E_0-\hbar\Omega)/s_{e\Gamma h'}}{\sqrt{(E_0-\hbar\omega)+(\hbar\omega-E_0-\hbar\Omega)/s_{e\Gamma h'}}}-2\right\}. \tag{A16}$$

APPENDIX B: CHOICE OF MATERIAL PARAMETERS

In this Appendix we discuss how we arrived at those material parameters listed in Table I that could not be taken directly from the literature, in most cases because they were measured at low temperatures. We then explain how, starting with the available data at low temperatures, one can estimate the corresponding values at our experimental temperature of 301 K.

1. Lattice parameter and band gaps

For the cubic lattice parameter we use an expression of the form

$$a_0(T) = a_0(0) + \frac{\beta}{\exp(T_0/T) - 1}, \tag{B1}$$

where $a_0(0) = 5.6516\,\text{Å}$, $\beta = 1.315 \times 10^{-2}\,\text{Å}$, and $T_0 = 355.14\,\text{K}$. We obtain these parameters by fitting Eq. (B1) to the lattice constant calculated by using the value at room temperature and an integral of the thermal expansion data from Ma and Tse [57].

The temperature dependence of all needed band gaps in Ge was assumed to follow the Varshni law [48]:

$$E_t(T) = E_t(0) - \frac{\alpha T^2}{T_0 + T}. \tag{B2}$$

We used for the indirect gap $E_{\text{ind}}(0) = 0.742\,\text{eV}$, $\alpha = 4.8 \times 10^{-4}\,\text{eV/K}^2$, and $T_0 = 235\,\text{K}$. For the direct gap, we took $E_0(0) = 0.8911\,\text{eV}$, $\alpha = 5.82 \times 10^{-4}\,\text{eV/K}^2$, and $T_0 = 296\,\text{K}$. For the calculation of effective masses we also need the E_1 and $E_1 + \Delta_1$ gaps, corresponding to vertical transitions at the L point of the BZ, and the E_0' gap, the separation between the valence band and the p-antibonding states. We took their temperature dependence from Viña *et al.* [58]. The corresponding Varshni parameters for E_1 are $E_1(0) = 2.22\,\text{eV}$, $\alpha = 6.8 \times 10^{-4}\,\text{eV/K}^2$, and $T_0 = 240\,\text{K}$. For $E_1 + \Delta_1$, we use $E_1 + \Delta_1(0) = 2.42\,\text{eV}$, $\alpha = 6.8 \times 10^{-4}\,\text{eV/K}^2$, and $T_0 = 240\,\text{K}$. Finally, for E_0' we take $E_0'(0) = 3.159\,\text{eV}$, $\alpha = 3.6 \times 10^{-4}\,\text{eV/K}^2$, and $T_0 = 344\,\text{K}$.

2. Effective masses and momentum matrix element

The conduction band effective mass was obtained by Roth *et al.* [59] by analyzing magnetoabsorption experiments at 4.2 K. They find a value of $m_{e\Gamma} = 0.037\,\text{eV}$. A very similar value, $m_{e\Gamma} = 0.038\,\text{eV}$, was obtained by Aggarwal from stress-modulated magnetoreflectance [60]. We insert the experimental effective mass into Eq. (5) to obtain the low-temperature momentum matrix element $P^2/m = 12.64\,\text{eV}$, where we used $\Delta_0 = 0.297\,\text{eV}$ [60,61]. The momentum matrix element is proportional to $1/a_0$ [20], so that we use

$$\frac{P^2(T)}{m} = 12.64\,\text{eV} \times \frac{a_0^2(4.2\,\text{K})}{a_0^2(T)}. \tag{B3}$$

For the conduction band masses at the L minimum of the conduction band we start with the classic work of Dresselhaus, Kip, and Kittel (DKK) [30]. They report a transverse mass $m_\perp = 0.082m$ and a longitudinal mass $m_\parallel = 1.58m$ at 4 K. We assume the longitudinal mass to be independent of temperature. The transverse mass is written as [20]

$$\frac{1}{m_\perp} = \frac{1}{m} + \left(\frac{\bar{P}}{m}\right)^2 \left(\frac{1}{E_1} + \frac{1}{E_1 + \Delta_1}\right). \tag{B4}$$

By fitting the experimental value at 4 K, we find $\bar{P}^2/m = 12.96\,\text{eV}$, so that $\bar{P}$ is very similar to P^2, as expected on theoretical grounds [20]. For the temperature dependence we then use

$$\frac{\bar{P}^2(T)}{m} = 12.96\,\text{eV} \times \frac{a_0^2(4\,\text{K})}{a_0^2(T)}. \tag{B5}$$

By combining Eq. (B5) with the temperature dependence of E_1 and $E_1 + \Delta_1$, we can obtain the transverse mass in Eq. (B4) at any temperature.

The valence bands display a significant level of warping. Effective masses can be introduced as suitable angular averages. In spherical coordinates, the energy dispersion can be written as [30,62]

$$E_v(\boldsymbol{k}) = \left(\frac{\hbar^2 k^2}{2m}\right)\{A \pm [B^2 + C^2(\sin^4\theta\sin^2\varphi\cos^2\varphi + \sin^2\theta\cos^2\theta)]^{1/2}\}, \tag{B6}$$

where the parameters A, B, and C were introduced by DKK [30]. The masses that appear in the absorption coefficient expressions are elevated to the 3/2 power, corresponding to the density of states. Accordingly, we define the angular-averaged effective masses as

$$m_h^{3/2} = \left(\frac{m}{|A|}\right)^{3/2} \frac{1}{4\pi} \int_\Omega \frac{d\Omega}{[1 \pm \sqrt{(B/A)^2 + (C/A)^2(\sin^4\theta\sin^2\varphi\cos^2\varphi + \cos^2\theta\sin^2\theta)}]^{3/2}}, \tag{B7}$$

where the minus sign leads to the heavy-hole mass m_{lh} and the plus sign to the light-hole mass m_{lh}. The DKK parameters that best describe the 4 K data are $A = -13.38$, $B = -8.48$, and $|C| = 13.14$. To obtain values appropriate for room temperature, we use the expressions [20]

$$\begin{aligned} A &= 1 - \frac{2}{3}\left[\frac{P^2}{mE_0} + \frac{2Q^2}{mE_0'}\right], \\ B &= \frac{2}{3}\left[-\frac{P^2}{mE_0} + \frac{Q^2}{mE_0'}\right], \\ |C|^2 &= \frac{16P^2Q^2}{3m^2E_0E_0'} + \Delta, \end{aligned} \tag{B8}$$

where the matrix element Q is defined in Ref. [20]. The equation for $|C|^2$ in Ref. [20] lacks the additive term Δ that appears in (B8). However, we find that this term is needed for an exact match of the low-temperature A, B, C experimental values. This is because the theory leading to Eq. (B8) relies on a number of simplifying approximations. However, since we are only interested in estimating the temperature dependence of the DKK parameters, we expect this theory to provide a good account of this dependence if we adjust the three parameters P, Q, and Δ for an exact match of the low-temperature DKK parameters. This leads to $P^2/m = 13.964\,\text{eV}$ [slightly different from the value in Eq. (B5) that provides the best fit for the conduction band effective mass], $Q^2/m = 9.287\,\text{eV}$, and $\Delta = -73.1$. We then assume that the temperature dependence of P^2 and Q^2 is given by Eq. (B5) and that the parameter Δ is independent of temperature. These values are inserted into Eq. (B8) (combined with the temperature dependence of E_0 and E_0') to obtain the DKK parameters at any temperature. At 301 K, our temperature of interest, we find $A = -14.55$, $B = -9.58$, and $|C| = 14.25$.

[1] J. Noffsinger, E. Kioupakis, C. G. Van de Walle, S. G. Louie, and M. L. Cohen, Phys. Rev. Lett. **108**, 167402 (2012).
[2] M. Zacharias, C. E. Patrick, and F. Giustino, Phys. Rev. Lett. **115**, 177401 (2015).
[3] M. Zacharias and F. Giustino, Phys. Rev. B **94**, 075125 (2016).
[4] G. Greene-Diniz, J. C. Abreu, and M. Grüning, Comput. Mater. Sci. **149**, 115 (2018).
[5] R. L. Hartman, Phys. Rev. **127**, 765 (1962).
[6] W. C. Dash and R. Newman, Phys. Rev. **99**, 1151 (1955).
[7] G. Macfarlane, T. McLean, J. Quarrington, and V. Roberts, Phys. Rev. **108**, 1377 (1957).
[8] J. I. Pankove and P. Aigrain, Phys. Rev. **126**, 956 (1962).
[9] J. Liu, X. Sun, R. Camacho-Aguilera, L. C. Kimerling, and J. Michel, Opt. Lett. **35**, 679 (2010).
[10] J. Michel, J. Liu, and L. C. Kimerling, Nat. Photonics **4**, 527 (2010).
[11] J. Mathews, R. Roucka, J. Xie, S.-Q. Yu, J. Menéndez, and J. Kouvetakis, Appl. Phys. Lett. **95**, 133506 (2009).
[12] S. Wirths, R. Geiger, N. von den Driesch, G. Mussler, T. Stoica, S. Mantl, Z. Ikonic, M. Luysberg, S. Chiussi, J. M. Hartmann *et al.*, Nat. Photon. **9**, 88 (2015).
[13] J. Menéndez, M. Noël, J. C. Zwinkels, and D. J. Lockwood, Phys. Rev. B **96**, 121201 (2017).
[14] R. J. Elliott, Phys. Rev. **108**, 1384 (1957).
[15] T. Nishino, M. Takeda, and Y. Hamakawa, J. Phys. Soc. Jpn. **37**, 1016 (1974).
[16] A. Frova, G. A. Thomas, R. E. Miller, and E. O. Kane, Phys. Rev. Lett. **34**, 1572 (1975).
[17] M. Altarelli and N. O. Lipari, Phys. Rev. Lett. **36**, 619 (1976).
[18] N. O. Lipari and M. Altarelli, Phys. Rev. B **15**, 4883 (1977).
[19] M. Rohlfing and S. G. Louie, Phys. Rev. B **62**, 4927 (2000).
[20] P. Y. Yu and M. Cardona, *Fundamentals of Semiconductors: Physics and Materials Properties* (Springer-Verlag, Berlin, 1996).
[21] M. Dressel and G. Grüner, *Electrodynamics of Solids: Optical Properties of Electrons in Matter* (Cambridge University Press, Cambridge, 2002).
[22] S. L. Chuang, *Physics of Optoelectronic Devices*, Wiley Series in Pure and Applied Optics (Wiley, New York, 1995).
[23] F. Szmulowicz, Phys. Rev. B **28**, 5943 (1983).
[24] B. K. Ridley, *Quantum Processes in Semiconductors* (Oxford University Press, Oxford, 1999).
[25] X. Q. Zhou, H. M. Vandriel, and G. Mak, Phys. Rev. B **50**, 5226 (1994).
[26] G. Li, A. Goñi, K. Syassen, and M. Cardona, Phys. Rev. B **49**, 8017 (1994).
[27] S. Krishnamurthy and M. Cardona, J. Appl. Phys. **74**, 2117 (1993).
[28] V. G. Tyuterev, S. V. Obukhov, N. Vast, and J. Sjakste, Phys. Rev. B **84**, 035201 (2011).
[29] F. Murphy-Armando and S. Fahy, J. Appl. Phys. **110**, 123706 (2011).
[30] G. Dresselhaus, A. Kip, and C. Kittel, Phys. Rev. **98**, 368 (1955).
[31] J. Halpern and B. Lax, J. Phys. Chem. Solids **26**, 911 (1965).
[32] R. Aggarwal, M. Zuteck, and B. Lax, Phys. Rev. **180**, 800 (1969).
[33] G. Nilsson and G. Nelin, Phys. Rev. B **6**, 3777 (1972).
[34] J. M. Hinckley and J. Singh, J. Appl. Phys. **76**, 4192 (1994).
[35] W. Trzeciakowski, J. Martínez-Pastor, and A. Cantarero, J. Appl. Phys. **82**, 3976 (1997).
[36] O. Madelung, *Physics of Group IV Elements and III-V Compounds* (Springer-Verlag, Berlin, 1982), Vol. 17a.
[37] O. Madelung, *Introduction to Solid State Theory*, Springer Series in Solid-State Sciences (Springer, Berlin, 1978).
[38] E. N. Economou, *Green's Functions in Quantum Physics*, 2nd ed., Springer Series in Solid-State Sciences Vol. 7 (Springer, Berlin, 1983).
[39] L. Hostler, J. Math. Phys. **5**, 591 (1964).
[40] G. D. Mahan, Phys. Rev. **170**, 825 (1968).
[41] R. M. Martin, Phys. Rev. B **4**, 3676 (1971).
[42] N. F. Mott and H. S. W. Massey, *The Theory of Atomic Collisions*, 3rd ed., The International Series of Monographs on Physics (Oxford University Press, Oxford, 1965).
[43] V. R. D'Costa, Y. Fang, J. Mathews, R. Roucka, J. Tolle, J. Menéndez, and J. Kouvetakis, Semicond. Sci. Technol. **24**, 115006 (2009).
[44] http://ispoptics.com.
[45] www.substrates.umicore.com.
[46] J. C. Zwinkels and D. S. Gignac, Appl. Opt. **31**, 1557 (1992).
[47] J. C. Zwinkels, M. Noël, and C. X. Dodd, Appl. Opt. **33**, 7933 (1994).
[48] Y. P. Varshni, Physica (Amsterdam) **34**, 149 (1967).
[49] S. C. Jain and D. J. Roulston, Solid-State Electron. **34**, 453 (1991).
[50] D. V. Seletskiy, R. Epstein, and M. Sheik-Bahae, Rep. Prog. Phys. **79**, 096401 (2016).
[51] C. Xu, J. D. Gallagher, C. L. Senaratne, J. Menéndez, and J. Kouvetakis, Phys. Rev. B **93**, 125206 (2016).
[52] C. C. Kim, J. W. Garland, H. Abad, and P. M. Raccah, Phys. Rev. B **45**, 11749 (1992).

[53] J. D. Gallagher, C. L. Senaratne, J. Kouvetakis, and J. Menéndez, Appl. Phys. Lett. **105**, 142102 (2014).
[54] W. P. Dumke, M. R. Lorenz, and G. D. Pettit, Phys. Rev. B **5**, 2978 (1972).
[55] P. Würfel, S. Finkbeiner, and E. Daub, Appl. Phys. A **60**, 67 (1995).
[56] G. Grzybowski, R. Roucka, J. Mathews, L. Jiang, R. Beeler, J. Kouvetakis, and J. Menéndez, Phys. Rev. B **84**, 205307 (2011).
[57] Y. Ma and J. S. Tse, Solid State Commun. **143**, 161 (2007).
[58] L. Viña, S. Logothetidis, and M. Cardona, Phys. Rev. B **30**, 1979 (1984).
[59] L. M. Roth, B. Lax, and S. Zwerdling, Phys. Rev. **114**, 90 (1959).
[60] R. L. Aggarwal, Phys. Rev. B **2**, 446 (1970).
[61] D. E. Aspnes, Phys. Rev. B **12**, 2297 (1975).
[62] S. Rodríguez-Bolívar, F. M. Gómez-Campos, and J. E. Carceller, Semicond. Sci. Technol. **20**, 16 (2005).